Soft Magnetic Materials and Applications

Frédéric Mazaleyrat

1

Soft Magnetic Materials and Applications

Frédéric Mazaleyrat

SATIE, CNRS, École normale supérieure Paris-Saclay, 4 avenue des sciences, 91 190 Gif-sur-Yvette, France mazaleyr@satie.paris-saclay.fr

Abstract. A great variety of soft magnetic material has been developed with the aim of enhancing the magnetization, increasing the permeability, controlling the hysteresis loop shape or raising the working frequency while in all cases decreasing the magnetic losses. Besides the physical considerations, material shaping and cost are important parameters. It is thus not surprising to see that despite natural selection, hundreds of materials of very different natures (metallic, ceramic, glass) and properties remain on the market. Choosing the right material for a specific application is often a tricky compromise and, too often, a question of industrial culture. This chapter aims at helping the user to make the best choice possible and gives some keys to improving device design. The first part is devoted to magnetic losses, giving the most-used models in the low-frequency non-linear regime and the high frequency linear regime. The following section describes the different families of materials: low-alloyed steels, iron-cobalt alloys, iron-nickel alloys, amorphous and nanocrystalline alloys and soft ferrites. In each section, the fabrication process is described and tables of typical properties of most common materials are given. Finally there is a table of applications and matching materials.

Contents

1.1 Losses in soft magnets

From his work on thermodynamics and magnetism, Lord Kelvin proposed that any change in magnetization should be accompanied by dynamic losses and heat release or absorption – an effect that was later discovered and named magnetocaloric effect by Pierre Weiss. Early work of Cazin in this direction has shown that change in magnetization at constant temperature always produces heat [16], but due to the geometry of the system and the frequency of magnetization switching, this was due essentially to eddy currents. In 1881 Warburg proved that this heating was not only due to dynamic effects [38] but to some kind of friction too, which was confirmed independently the same year by Ewing [18] who developed the first $B(H)$ loop tracer. He showed that the loop area is identical to heat release and named the phenomenon hysteresis. Immediately, it was recognized that the hysteresis depends on both flux density and frequency and that below a certain frequency, the area and shape of the loop depends no more on the frequency. This floor value of the losses is known as *hysteresis loss*hysteresis loss. The concept of loss separation was proposed by Braisford [15] as the sum of the hysteresis loss, P_{hy} and eddy current loss, P_{ec}. The difference between measured iron loss P_{Fe} and these two components was called anomalous loss $P_{an} = P_{Fe} - P_{hy} - P_{ec}$. The physical origin of what we rather called excess loss P_{ex} will be found long time later and properly embedded in a reliable theory only in 1988 (see sec. 1.1.2.) In general, losses have to be expressed in specific units, either power or energy per unit volume or mass depending on customs of different communities. Eventually in linear regime, losses can be expressed as a function of the loss angle $\delta = \frac{\pi}{2} -$ phase lag between voltage and current. Usual units are :

- electrical machines $\mathrm{W \cdot kg^{-1}}$;
- power electronics $\mathrm{W \cdot m^{-3}}$ or $\mathrm{mW \cdot cm^{-3}}$;
- modelisation $\mathrm{J \cdot m^{-3}}$;
- electronics $\tan \delta$.

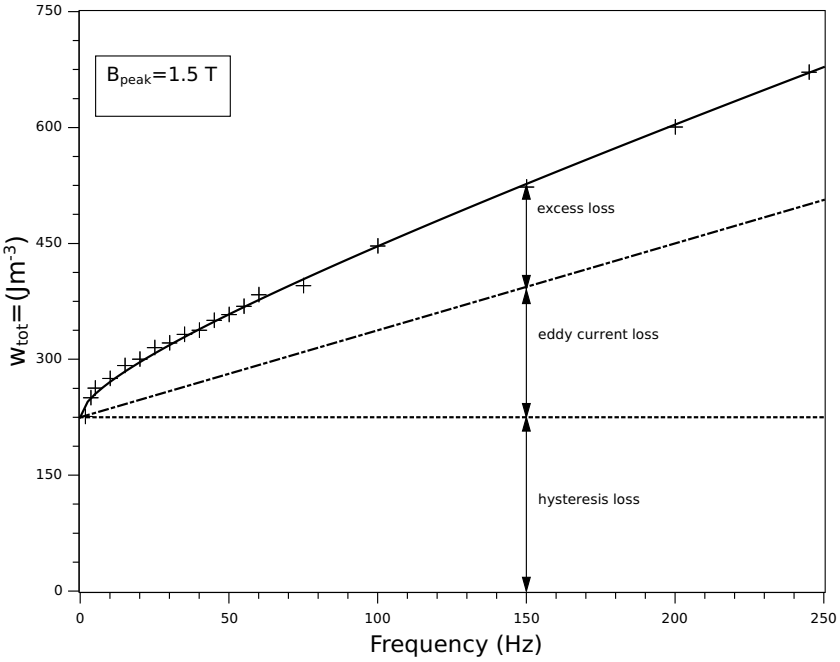

Fig. 1.1. Separation of losses in a 2.4 W/kg grade silicon steel. Lines correspond to the model and + to the experiment

The dependence of losses upon magnetization and frequency is rather complex and can hardly be modelled by explicit equations, however in a first approximation losses can be fitted using the separation principle and Steinmetz exponents in the following forms:

volume energy loss	volume power loss	mass power loss
Expressed in Jm^{-3}	Expressed in Wm^{-3}	Expressed in Wkg^{-1}
$W_h = k_0 B^2$	$\mathcal{P}_h = k_0 B^2 f$	$p_h = k_0 B^2 f/\rho$
$W_{cl} = k_1 B^2 f$	$\mathcal{P}_{cl} = k_1 B^2 f^2$	$p_{cl} = k_1 B^2 f^2/\rho$
$W_{ex} = k_2 B^m f^n$	$\mathcal{P}_{ex} = k_2 B^m f^{n+1}$	$p_{ex} = k_2 B^m f^{n+1}/\rho$

It must be however emphasized that only the classical term can be determined a priori. The other terms are determined from experiments. As it will be shown in §1.1.2 the exponents of the excess part are $n = 1/2$ and $m = 3/2$ in many cases, but this is not a general rule. In a limited range of induction and frequency, it is always possible to find an expression of losses like $P_{Fe} = kB^\eta f^\xi$ but this is only a fitting definitively free of physical sense.

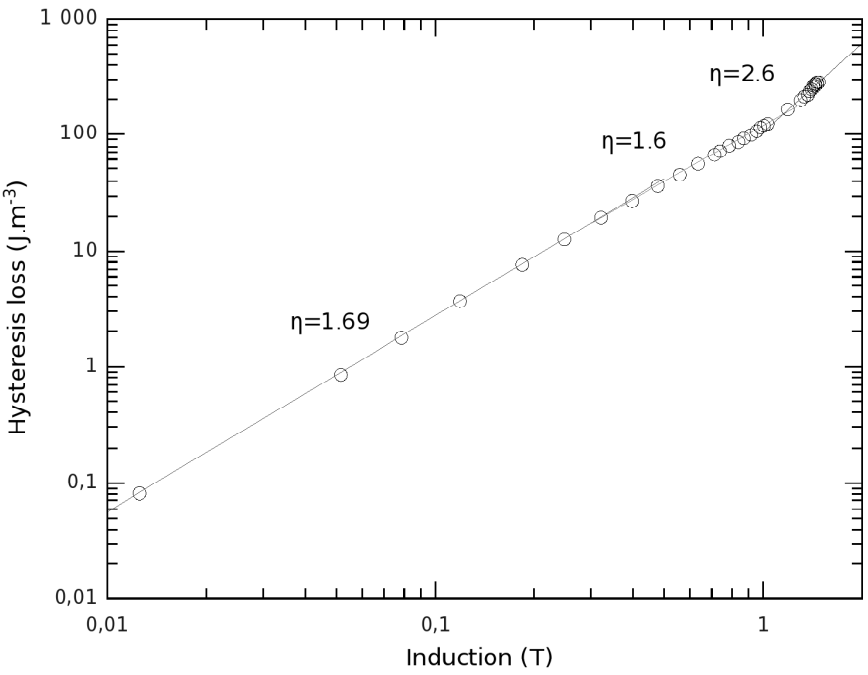

Fig. 1.2. Fitting of Stneimetz exponent in a non-oriented Fe-Si steel sheet

1.1.1 Hysteresis loss

Hysteresis loss is the most difficult loss term to model. At the end of the XIXth century, Rayleigh and Steinmetz proposed empirical models for hysteresis loss, and we must say that more than one century later, there is no better simple model. Since the 50's Preisach model has been developed and widely studied. It's based on the decomposition of the hysteresis loop in elementary loops (hysteron) defined by a coercive and a shift field. To compute Preisach distribution , its is necessary to record a great number of minor loops (or reversal curves) in order to sweep uniformly the whole area of the major loop. The distribution allows to compute any trajectory in the $M(H)$ plane, but finally, if it is useful for researchers to study the magnetization mechanisms in soft or even hard materials, it remain usually too complicated for implementation in an industrial software.The recovery of the distribution is not straightforward and would need developments out of the scope of this chapter, for more detail, the reader is invited to refer to the monumental "Science of hysteresis" [14]

1.1.2 Low frequency losses

Steinmetz model

The Steimetz model for hysteresis loss has actually no physical basis. It was discovered purely empirically in 1905 and written in the form kB^{η}. Plotting hysteresis losses vs induction in log-log scale allows to deduce the coefficient and the exponent, but the exact value of the exponent η depends somehow on the considered induction window as it is seen on Fig.1.2. As observed by Steinmetz, a value close to 1.6 is generally observed. This value can't be easily connected with the result of Rayleigh because the latter is expressed as a function of H and because the permeability is not constant. At higher induction, the exponent increases over 2 and then drops to zero in the reversibility region of the major loop (close to saturation) [10]. In average in a large range of induction, an exponent 2 is usually a good approximation but the error can be up to 100%. However, in some cases, hysteresis loss can be a minor component of the loss.

Rayleigh loops

In the small signal regime, i.e. when $B \ll \mu_0 M_S$, Rayleigh observed linear and quadratic behaviours of permeability and initial magnetization curve respectively :

$$\mu = \mu_i + \nu H \; and \; B = \mu_i H + \nu H^2 \tag{1.1}$$

where μ_i is the initial permeability and η is an empirical constant. Starting from a non-zero field H_m the upper or lower branch of the hysteresis loops can be described from this law in the form:

$$B = (\mu_i + \nu H_m)H \pm \frac{1}{2}\nu(H_m^2 - H^2) \tag{1.2}$$

from which the area of the loop can be deduced:

$$W_h = \frac{4}{3}\nu H_m^3 \; or \; \mathcal{P}_h = \frac{4}{3}\nu H_m^3 f \tag{1.3}$$

To write the loss dependence on B, one has to solve the second order equation (1.1) which single physical solution can be introduced in (1.3):

$$W_h = \frac{\mu^3}{6\nu^3}\left[\sqrt{1 + \frac{4\nu B}{\mu^2}} - 1\right] \tag{1.4}$$

If $\mu^2 \gg 4\nu B$:

$$W_h = \frac{4}{3}\sqrt{\frac{\mu^3}{\nu}}B^{3/2} \tag{1.5}$$

we end up with a Steinmetz exponent of 1.5, which is very close to the experimental one.

This law is pretty much simple but its validity is limited to $B \ll J_S/10$. Such low induction in practice are used only at high frequency, i.e. several tens or hundred of kHz. Under these conditions, hysteresis losses are negligible compared to eddy currents in metals, so this law is more useful in practice for ferrites. Experience shows that Rayleigh law is well obeyed in ferrites up to 25 mT and over 100 kHz in highly resistive NiZn type ferrites (see e.g. [1])

Eddy currents

When any conductive material is submitted to AC magnetic field, eddy currents are created inside in such a way they produce a counter field. This contribution to losses will be added to the hysteresis (DC) component of the losses. It's nature is purely Maxwellian and refers to an isotropic and homogeneous material at macroscopic scale, which is not realistic for ferromagnetic materials because of the domain structure. However, in certain conditions, i.e. if domains are small compared to dimensions of the sample and isotropically distributed, or, if the domain walls move little compared to domain width (Rayleigh regime), eddy currents are as if the material is magnetically homogeneous.

Classical losses

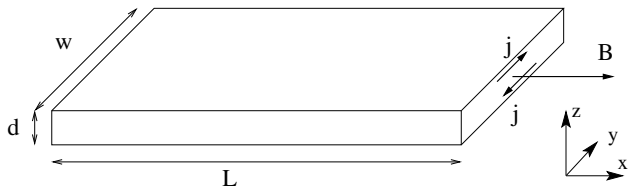

Fig. 1.3. Geometry of the problem for a thin sheet, eddy currents are everywhere perpendicular to **B** and parallel to the surface

This term refers to eddy current loss in the approximation of a weak skin effect, i.e. when the magnetic field produced by eddy currents in reaction to the exciting field, H_{ex} is very small. In other worlds, the inductive reaction has no significant effect on the flux density B which is considered uniform in space. From Maxwell-Faraday equation

$$\nabla \times \mathbf{E} = -\frac{\partial \mathbf{B}}{\partial t} \tag{1.6}$$

and looking at the geometry of the problem Fig. 1.3 with $L, w \gg d$, one can see that (i) the flux density has only one component along x depending only on time, (ii) the current density, $\mathbf{j}$ has a single y component independent on x

and y, so that the electrical field has the same symmetry through Ohm's law $\mathbf{j} = \sigma\mathbf{E}$.

$$\frac{\partial E_y}{\partial z} = \frac{\partial B_x}{\partial t} \Rightarrow E_y(t,z) = \frac{\partial B_x}{\partial t} z + K \tag{1.7}$$

Because of the symmetry, $E_y = 0$ in the middle –where we advantageously locate the origin– $K = 0$. The power dissipated in the volume can be obtained from the integral on the half thickness:

$$P_{cl}(t) = \int_V \sigma E_y^2 \mathrm{d}V = 2Lw\sigma \left(\frac{\partial B_x}{\partial t}\right)^2 \int_0^{d/2} z^2 \mathrm{d}z \tag{1.8}$$

and dividing by the volume dwL, the instantaneous power per unit volume is derived,

$$\mathcal{P}_{cl}(t) = \frac{1}{12}\sigma \left(\frac{\partial B_x}{\partial t}\right)^2 d^2 \tag{1.9}$$

Getting the mean power density requires to define the function $B_x(t)$. Usually in low frequency applications such as AC machines and transformers, as well as in standard characterization conditions, the induction is sinusoidal. The average of a squared sinus being $\frac{1}{2}$, we end up with the well known formula, where B_p denotes the peak value of the induction:

$$\mathcal{P}_{cl}^{sin} = \frac{\pi^2}{6}\sigma f^2 B_p^2 d^2 \tag{1.10}$$

By opposition, in power electronics, the voltage has often a square wave form, so $B(t)$ is triangular. In this case, the time derivative of B is constant over a half period so it's value is $4fB_p$ for an induction swing of $2B_p$ and one gets:

$$\mathcal{P}_{cl}^{tri} = \frac{4}{3}\sigma f^2 B_p^2 d^2 \tag{1.11}$$

It is easy to see that the classical losses are 23% lower for triangle waveform compared to sinus for the same B_p.

Skin effect

When the low frequency condition is not satisfied, interaction between electrical and magnetic fields must be introduced and Maxwell-Ampère equation can be combined with Ohm's law as $\nabla \times \mathbf{H} = \mathbf{j} = \sigma\mathbf{E}$. Further, the permeability is introduced

$$\nabla \times (\nabla \times \mathbf{H}) = \nabla \times \mathbf{j} = \sigma \nabla \times \mathbf{E} = -\sigma \frac{\partial \mathbf{B}}{\partial t} = -\sigma\mu \frac{\partial \mathbf{H}}{\partial t} \tag{1.12}$$

Using the property $\nabla \times (\nabla \times \mathbf{H}) = \Delta\mathbf{H} - \nabla(\nabla \cdot \mathbf{H}) = \Delta\mathbf{H}$, one finally gets the diffusion equation:

$$\Delta\mathbf{H} = -\sigma\mu \frac{\partial \mathbf{H}}{\partial t} \tag{1.13}$$

In the geometrical conditions of Fig. 1.3

$$\frac{\partial^2 H_x(z,t)}{\partial z^2} = \sigma\mu\frac{\partial H_x(z,t)}{\partial t} \tag{1.14}$$

In sinusoidal regime, this differential equation can be rewritten in complex form

$$\frac{\partial^2 h(z)}{\partial z^2} = i\sigma\mu\omega h_x(z) \tag{1.15}$$

where the peak value of the field in the direction x is $\sqrt{2}h$. A solution of this equation can be found in the form of either exponential or hyperbolic functions. In this case, because of the symmetry, the surface field is equal to the applied field $h(d/2) = h(-d/2) = h_a$ so the hyperbolic solution has the simple form $h_x(z) = A\cosh(\mathbf{k}z)$ where the complex number $\mathbf{k}$ is define as $\mathbf{k}^2 = i\sigma\mu\omega$. It is usually convenient to write $\mathbf{k} = (1+i)/\delta$, where the quantity δ, homogeneous with a length, is called the penetration or skin depth:

$$\delta = \sqrt{\frac{2}{\sigma\mu\omega}} \tag{1.16}$$

so an hyperbolic solution is easily found taking into account the boundary conditions:

$$h(z) = h_a\frac{\cosh(\mathbf{k}z)}{\cosh(d/2)} \tag{1.17}$$

The RMS value of the field is obtained by calculating the square root of the conjugate product

$$h(z) = h_a\sqrt{\frac{\cosh(2z/\delta) + \cos(2z/\delta)}{\sinh(d/\delta) + \sin(d/\delta)}} \tag{1.18}$$

With the present symmetry of the problem, the RMS value of the y single component of the current density is written from Maxwell-Ampère equation as

$$j(z) = \frac{\mathrm{d}h}{\mathrm{d}z} = \frac{\sqrt{2}}{\delta}h_a\sqrt{\frac{\cosh(2z/\delta) - \cos(2z/\delta)}{\cosh(d/\delta) + \cos(d/\delta)}} \tag{1.19}$$

The volumetric Joule losses produced by eddy currents in the sample are obtained by integration over the thickness divided by the volume

$$\mathcal{P}_{ec} = \frac{1}{\sigma e}\int_{-d/2}^{d/2}\left|\underline{j_y}(z)\right|^2\mathrm{d}z \tag{1.20}$$

$$\mathcal{P}_{ec} = \frac{2}{\sigma e\delta}H_a^2\frac{\sinh(d/\delta) - \sin(d/\delta)}{\cosh(d/\delta) + \cos(d/\delta)}, \tag{1.21}$$

where H_a is the peack value of the applied (external) field.

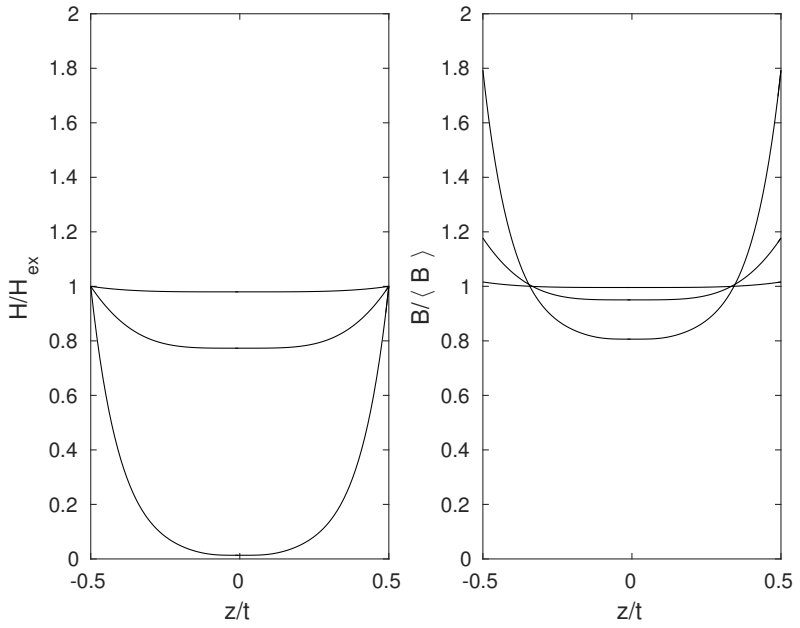

Fig. 1.4. Profile of the field H across the thickness reduced to excitation field and profile of B reduced to the space averaged induction for δ/d =1, 0.5, 0.1. B is calculated in the linear case, clearly this model is not adapted for small δ/d when $\langle B\rangle$ is close to J_S.

However, in many cases – electrical machines, transformers, standard measurements – not the excitation field is the driving force, but the induction. Considering a constant permeability in the whole material, the average induction over the cross section is written knowing the value of B at the surface $(x, y, \pm e/2)$:

$$\langle B(z)\rangle = B_{surf}\frac{1}{d}\int_{-d/2}^{d/2}\frac{\cosh(\mathbf{k}z)}{\cosh(\mathbf{k}d/2)}\mathrm{d}z = B_{surf}\frac{\tanh(\underline{\mathbf{k}}d/2)}{(\mathbf{k}d/2)} \tag{1.22}$$

The quantity H_{ex} in (1.21) is substituted by $\langle B(z)\rangle/\mu_0\mu_R$ and calculating the conjugate quantity product of the hyperbolic term yields the following reduction:

$$\mathcal{P}_{cl} = \frac{\pi f d}{2\delta}\frac{\langle B\rangle^2}{\mu_0\mu_R}\cdot\frac{\sinh\left(\frac{d}{\delta}\right)-\sin\left(\frac{d}{\delta}\right)}{\cosh\left(\frac{d}{\delta}\right)-\cos\left(\frac{d}{\delta}\right)} \tag{1.23}$$

It must be emphasized that this formula is valid only when the permeability is constant. This condition is a strong restriction when $\delta \ll d$ because the field at

the surface is much stronger than in the center (see Fig.1.4). As a consequence even if $\langle B \rangle \ll J_S$ the sample may be saturated close to the surface. In this case, there is no analytical solution, specific and time consuming algorithms must be used (see [17] for more details.)

Excess loss

The Pry and Bean Model

The well known Pry and Bean model was developed to study the eddy current losses generated by the movement of domain walls in a periodic array of infinite slab domains. Let's call $2L$ the width of a domain, d the thickness of the slabs and and x the instantaneous position of the wall this respect to the zero net magnetization of the array ($x = 0$ for $\langle B \rangle = 0$). The relation between the instantaneous magnetization and the position of the wall is thus $J(t) = \frac{1}{L} x(t) J_S$. Taking into account the boundary conditions the solution can be express in terms of series expansion of hyperbolic terms. The resolution is rather complicated, but details can be found in the classical paper [29]. For convenience we adopted the following form of the time dependant losses per unit volume [11]:

$$\mathcal{P}_{PB}(t) = \frac{\sigma}{2Ld} \left(\frac{\partial \phi}{\partial t} \right)^2 \frac{4}{\pi^4} \sum_{odd\ n} \frac{1}{n^3} \left[\coth\left(n\pi \frac{L+x}{d} \right) + \coth\left(n\pi \frac{L-x}{d} \right) \right] \tag{1.24}$$

If the domain are very thin ($2L \ll d$) $\coth(x) \simeq 1/x$ and one can find the classical result of (1.9). On the over side, if $2L \gg d$ the coth terms are close to unity and (1.24) is reduced to:

$$\mathcal{P}_{PB}(t) = \frac{\sigma G}{2Ld} \left(\frac{\partial \phi}{\partial t} \right)^2 \tag{1.25}$$

by writing $\frac{4}{\pi^4} \sum\limits_{odd\ n} \frac{1}{n^3} = G = 0.1356$. In grain oriented Fe-Si sheets, the latter condition is rather justified since $2L > 2$ mm$/d = 0.24$ mm and very well justified for longitudinal field annealed amorphous ribbons $2L > 5$ mm$/d = 0.02$ mm.

Bertotti's model

The basis of Bertotti's model (see [12] and [11] for more details) is the application of Pry and Bean model to a system composed of slab domain regions randomly oriented in space. From statistical arguments, Bertotti has shown that in this case the total dynamic losses is equivalent to the sum of classical eddy currents superimposed with eddy currents generated by periodic slab domains parallel to the field $\mathcal{P}_{dyn}(t) = \mathcal{P}_{cl}(t) + \mathcal{P}_{PB}(t)$. This validates theoretically the concept of loss separation $\mathcal{P}_{Fe} = \mathcal{P}_{hy} + \mathcal{P}_{cl} + \mathcal{P}_{ex}$, where the excess loss is the time average of 1.25:

$$\mathcal{P}_{ex} = \frac{\sigma G}{2Ld}\left\langle\left(\frac{\partial\phi}{\partial t}\right)^2\right\rangle = \frac{\sigma G}{2Ld}(1+\alpha)\left\langle\frac{\partial\phi}{\partial t}\right\rangle^2 \tag{1.26}$$

where α is a form factor depending only the flux waveform. It is now interesting to introduce the notion of excess field which is the supplementary field necessary to obtain the desired change in magnetization due to the dynamical movement of domain walls:

$$\mathcal{P}_{ex} = H_{ex}\frac{\partial J}{\partial t} \tag{1.27}$$

It is now easy to substitute the flux by the magnetization $J = \phi/2Ld$ in this expression and to equate with (1.26) and to get:

$$H_{ex} = 2Ld\sigma G(1+\alpha)\frac{\partial J}{\partial t} \tag{1.28}$$

Let now introduce the width of the sheet, ℓ, the area of the cross section perpendicular to the field is $S = \ell d$ and the number of domain walls in this section is $n_w = \ell/2L$, now we have:

$$H_{ex} = \sigma G(1+\alpha)\frac{S}{n_w}\cdot\frac{\partial J}{\partial t} = \frac{\sigma G S}{n}\cdot\frac{\partial J}{\partial t} \tag{1.29}$$

where we substituted $n = \frac{n_w}{1+\alpha}$ to simplify. Thus, n is no more the real number of domain wall but an effective number depending on the waveform. This is actually not a problem since n, also called the number of magnetic objects, will be identified from loss measurements using a given waveform. However, is is reasonable to think that the number of active magnetic object will depend on the excess field (larger excess field will activate more magnetic objects), so at first order one can write:

$$n = n_0 + \frac{H_{ex}}{V_0} \tag{1.30}$$

where n_0 is the number of active objects at zero field, and V_0 the field necessary to activate one more object over the total number of magnetic objects available N_0. Physically speaking, a magnetic object can be a domain or a set of domain moving coherently, in other words, a crystallographic grain. Introducing (1.30) in (1.29) leads to the second order equation

$$n_0 H_{ex} + n_0\frac{H_{ex}^2}{V_0} = \sigma G S\frac{\partial J}{\partial t} \tag{1.31}$$

which admits one physical solution over the to mathematical

$$H_{ex} = \frac{-n_0 V_0 + \sqrt{n_0^2 V_0^2 + 4V_0\sigma G S\frac{\partial J}{\partial t}}}{2} \tag{1.32}$$

The excess loss can now be expressed from (1.26) after factorization

$$\mathcal{P}_{ex} = \frac{n_0 V_0}{2}\left(\sqrt{1+\frac{4\sigma GS}{n_0^2 V_0}\cdot\frac{\partial J}{\partial t}}-1\right)\frac{\partial J}{\partial t} \tag{1.33}$$

Deducing the parameters of the model from measurement is not straightforward but there is an abundant literature describing the method. By chance in many case, particularly small grain non oriented materials, both n_0 and V_0 are relatively small, so (1.33) is reduced to

$$\mathcal{P}_{ex} = \sqrt{\sigma V_0 GS}\left(\frac{\partial J}{\partial t}\right)^{\frac{3}{2}} \tag{1.34}$$

So obviously in this case the parameter V_0 is the most important from physical point of view. Indeed, in small grain materials, N_0 can be understood as the number of grains of average diameter D in the cross section and:

$$V_0 \simeq \frac{2H_{hy}}{N_0} \tag{1.35}$$

where H_{hy}, the hysteresis field is defined from $\mathcal{P}_{hy}$ the same way the excess field is defined (see 1.26). So in principle this parameter is directly related to the micro-structure and the time dependants of the magnetization.

In the case of triangular flux waveform, the time derivative of the magnetization can be simply expressed on a half period as a function of the frequency and the peak magnetization $\frac{\partial J}{\partial t} = 4J_p f$, so (1.33) can be written in terms of power or energy per unit volume:

$$\mathcal{P}_{ex} = 8\sqrt{\sigma V_0 GS}J_p^{\frac{3}{2}} f^{\frac{3}{2}} \tag{1.36}$$

$$W_{ex} = 8\sqrt{\sigma V_0 GS}J_p^{\frac{3}{2}} f^{\frac{1}{2}} \tag{1.37}$$

so we end up with the famous square root frequency dependence of the excess losses observed experimentally by Brailsford [15]. The classical result of Bertotti (1.37) must be considered with caution:

- the approximation $n_0 = 0$ is not always verified, so (1.33) must be used;
- V_0 is an average over a cycle, so in principle, it increases appreciably with J_p since the number of magnetic object available for switching goes to zero close to saturation;
- in the case of sine waveform, the factor 8 in (1.37) should be replaced by 8.76 [8];
- if both n_0 and N_0 are large (1.33) can be approximated by $\mathcal{P}_{ex} = \frac{4\sigma GS}{n_0}J_p^2 f^2$;
- the decomposition is not possible for significant skin effect, in particular excess loss can appear negative at high induction due to the strong induction gradient in the lamination.

Typical example of square root dependence of the excess losses in non-oriented silicon steels is given in the left box of Fig.1.5 The difference between experimental point and the line at low field is due to the fact n_0 cannot be assumed exactly zero. The right box shows that V_0 depends on the peak induction and is not a constant as it is expected from (1.30). This however makes physical sense as explained above and can be related to Preisach distribution. This doesn't invalidate Bertotti's model but one have to make a choice between accuracy (that need determination of V_0 dependence on (J_p)) and simplicity (using an average V_0).

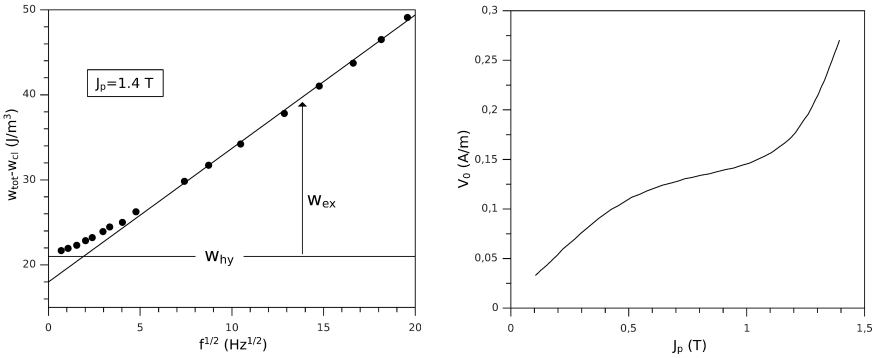

Fig. 1.5. Plot of losses as a function of square root frequency in non-oriented Fe-Si sheets used for determination of Bertotti's model parameters (left). V_0 parameter evolution with magnetization (rigth) after [8]

For accurate modelling of high frequency losses with skin effect, more complicated techniques must be used as in reference [10] based on dynamic Preisach model [13].

Rotational losses

Rotational losses are important in classical AC machines where the induction has usually a constant magnitude and a constant angular speed. It is however a simplified view because locally the induction locus can be rather ellipsoidal than circular. Also in three-phase transformers, at the junction between columns and yokes the induction has a direction depending on time. In the frame of this chapter, only the case of circular locus will be discussed.

Rotational eddy currents loss

Here again, the only part of the losses we can model easily is the eddy current part. In the case of a circular locus, $B(t) = B_p$ and $\theta = \Omega t$. Ferarris theorem

shows that any rotating field can be decomposed in two fixed direction time dependent perpendicular components:

$$B_x = B\cos\Omega t \text{ and } B_y = B\sin\Omega t \tag{1.38}$$

It follows immediately that

$$\mathcal{P}_{cl}^{R} = 2\mathcal{P}_{cl} \tag{1.39}$$

Rotational hysteresis loss

The most striking figure of rotational hysteresis loss is the fact they first increase with B at double speed compared to the hysteresis loss measured in a fixed direction, goes through a maximum around the inflexion point of the magnetization curve and drops to zero close to the saturation. This phenomenon discovered by Baily in 1896 seemed first to be inconsistent but soon became an strong argument in favour of Weber's molecular theory of magnetism saying that Ampère's molecular currents where permanent and that only the direction of the moments changes. Actually, today's interpretation is not so far: as the field is enough to saturate locally all grains (in other words to suppress domain walls) the magnetization is uniform and turns towards the field loss-less. Only the unavoidable eddy currents remains, because experience can hardly be done in real DC conditions. This is perfectly illustrated by the measurements shown Fig.1.6 where we see that the calculated classical loss curve intercepts the measured total loss curve.

Because evaluation of excess loss is time consuming and because they are usually small compared to other components, they are often neglected.

1.1.3 High frequency losses

From the previous sections, it can be concluded that magnetic power losses approximately goes with the square of B and an exponent of f between 1 and 2. As a consequence, reasonable losses at high frequency can be obtained only keeping a reasonable value of the $B \times f$ product, which means a very low value of B. In this case, the material works in the linear regime and its properties are advantageously represented in the form a complex permeability. An inductance can be modelled either by a parallel or series circuit, the later being the most common:

$$\underline{Z} = R + jL\omega = j\omega\left(L - i\frac{R}{\omega}\right) = j\omega\left(\frac{N^2\mu_0\mu_R A}{\ell} - i\frac{R}{\omega}\right) \tag{1.40}$$

where N is the number of turns of the coil, A and ℓ are the effective cross sectional area and length of the magnetic circuit. From this equation it is easy to identify the real part of the permeability and the imaginary part,

$$\underline{\mu} = \mu_R - j\frac{(r - R_0)\,\ell}{N^2\mu_0 S} = \mu' - j\mu'' \tag{1.41}$$

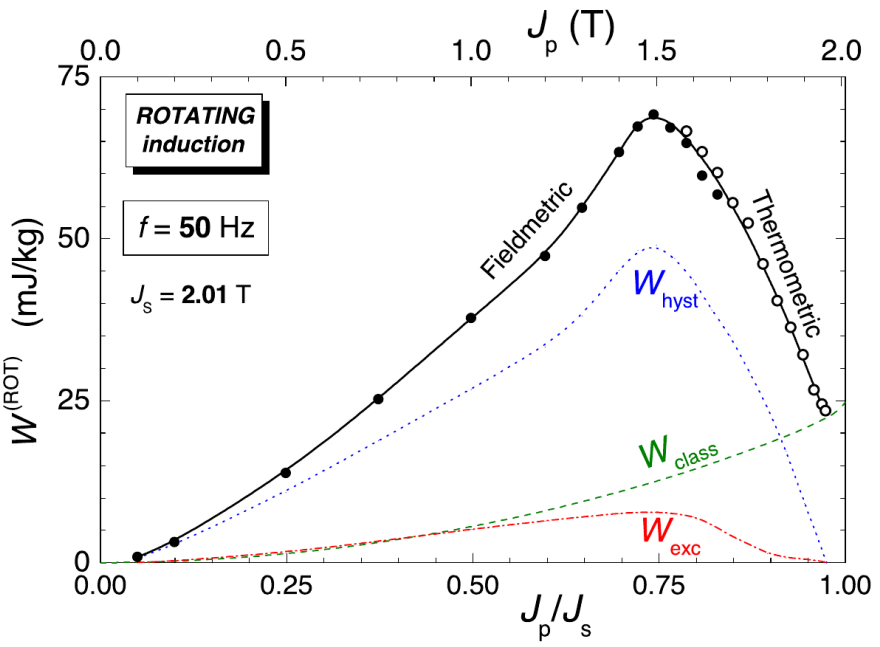

Fig. 1.6. Rotational losses measured at 50 Hz and separation of losses in NOSS [7]

where R_0 is the ohmic resistance of the coil and r is the series resistance standing for the iron loss. The loss factor is usually defined as:

$$\tan\delta = \mu''/\mu' \tag{1.42}$$

High frequency losses in metals

It is obvious that in the case of high frequency, losses goes with the higher frequency exponent term of the three components, namely, eddy current term in the case of magnetic conductors. In general, because of eddy currents, metallic magnetic materials are used in the form of thin ribbons or layers from several μm down to several nm, so this still corresponds to the usual thin foil approximation studied previously (see Fig.1.3).

If the excitation field is very small, the permeability can be considered more or less locally independent of H_{ex} and f, so the complex apparent permeability is simply the ratio between the average induction as defined in (1.23) and the field:

$$\underline{\mu} = \mu_S \frac{\tanh(\mathbf{k}^d/2)}{(\mathbf{k}^d/2)} \tag{1.43}$$

Getting an analytical expression of the real and imaginary parts of (1.43) is not straightforward, but any mathematical software will easily compute μ'

and μ'' knowing the main physical parameters: low frequency permeability, conductivity and thickness. The permeability spectra have two main features

- the static permeability $\mu_S = \lim_{f\to 0} \mu'(f)$
- the relaxation frequency $\max(\mu''(f)) = \mu''(f_R)$

and

$$f_R = \frac{4\rho}{\pi\mu_0\mu_S d^2} \tag{1.44}$$

so it is easily seen that the product $\mu_S f_R$ is a factor of merit independent of the permeability and proportional to ρ/d^2

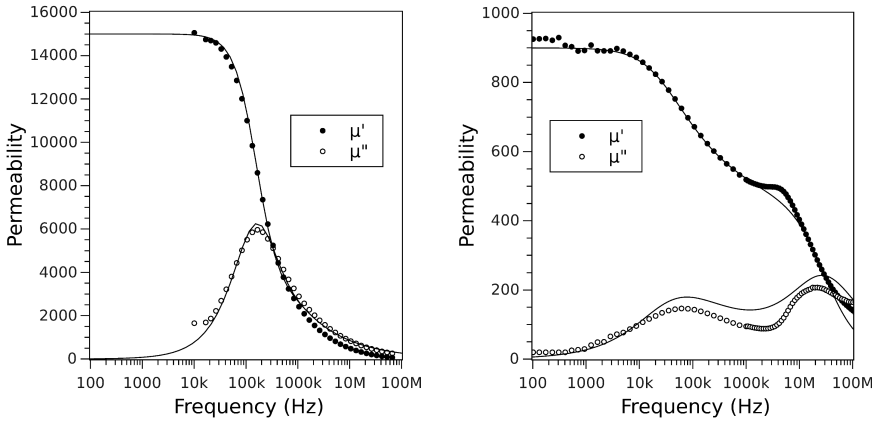

Fig. 1.7. Complex permeability spectra of different soft magnetic materials. Left, nanocrystalline wound core: points are experimental, line is computed using (1.43) using parameters measured independently (t=25μm, $\rho = 120 \cdot 10^{-6}$ Ωm). Right, ferrite showing double relaxation behaviour typical of material having bimodal grain size distribution: points are experimental, lines are fitted using the sum two terms with parameters $\alpha_1 = 0.5$, $\beta_1 = 0.65$, $f_{R1} = 30$ kHz, $\alpha_2 = 1$, $\beta_2 = 0.7$, $f_{R2} = 30$ MHz (1.45)

High frequency losses in insulators

The case of insulators is much more complicated than that of metals. Indeed, the exact mechanism producing magnetic losses is not clear and difficult to model. As a consequence, the first idea is to adopt Debye model where the mechanism of losses is analogous to dry friction. In other words the losses in terms of power are linearly dependent on frequency. Because in real materials there is always a distribution of local properties (the local permeability is strongly dependent on the grain size), there is nether a perfect Debye behavior, so the following model is often use:

$$\underline{\mu} = \frac{\mu_S}{(1 + (j^f/_{f_R})^\beta)^\alpha} \tag{1.45}$$

where the models are called

- Debye if $\alpha = \beta = 1$,
- Davidson-Cole if $\alpha < 1$ and $\beta = 1$
- Cole-Cole if $\beta < 1$ and $\alpha = 1$

This model when α and $\beta \neq 1$ are sometimes referred as non-integer derivative, but the reader must keep in mind that it's only a mathematical fitting. Some materials also show two distinct loss mechanisms (usually attributed to domain wall relaxation and spin resonance) which can be decomposed in two terms [36], but here again it's often mainly a fitting (see Fig.1.7). Also, ferrites sometimes show strong asymmetric resonance behaviour which cannot be properly modelled [31].

Interestingly, for a given ferrite composition, if the static permeability can be tuned by controlling grain size and porosity, the merit factor $\mu_S f_R$ is constant and strikingly for Ni-Zn properly processed it remains between 3 and 5 GHz. Moreover, if the frequency is far above f_R, (1.45) for $\alpha = \beta \approx 1$, becomes:

$$\underline{\mu} \to \frac{\mu_S f_R}{f} \tag{1.46}$$

this asymptotic behaviour is known as Snoeck's limit , it is applicable only for insulators (Ni-Zn, Mn-Mg ferrites, garnets), for Mn-Zn, additional eddy current loss has to be taken into account like in metals.

1.2 Iron and low carbon steels

Iron was the only soft material used until the very beginning of the XX^{th} century. For industrial applications, such as electrical motors and transformers, iron has usually two functions: magnetic and mechanical. From magnetic point of view, iron has a high induction, high permeability, but its conductivity is too high for efficient AC applications. For this reason, iron is today used only in DC applications such as pole pieces for lab electromagnets. The mechanical function of iron is very important because the magnetic core carries the coils in transformers and is subject to magnetic forces in machines or electromagnets. As a consequence, low carbon steel are usually preferred for DC application, whereas it can't be used in AC application because of the enhancement of the coercivity due to interstitial C atom in the BCC lattice of iron. The main application of low carbon steels as magnetic parts are: rotors of current excited synchronous machines and stators of DC machines. In power station turbo-generators and claw pole automobile generators, the rotor is made by forging. In the case of DC machines, the stator can be made

by stamping of thick sheet for several hundred watt machines and casting for bigger machines.

1.3 Electrical steels

1.3.1 Composition, processing and texture

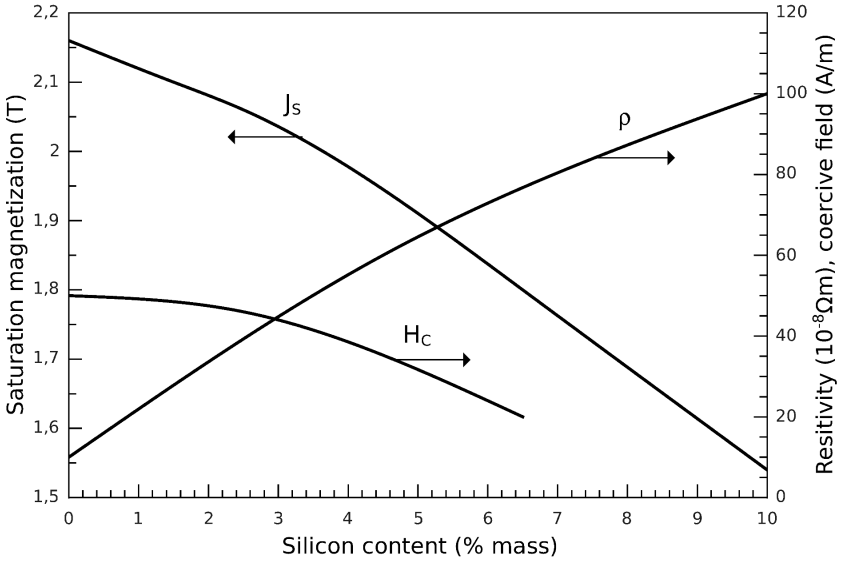

Fig. 1.8. Silicon dependence of room temperature saturation magnetization and resistivity of Fe-Si alloys. Coercivity is also given as a trend only since it depends on the manufacturing process.

Composition

In the beginning of the industrial era, metallurgists tried to reduce the carbon residue in iron to enhance its magnetic softness at the price of poor mechanical properties. In 1896, Hadfield fortuitously produced steel with a small percentage of silicon and observed strong enhancement of its mechanical hardness. By 1900 he measured its magnetic properties, showing that silicon not only improves iron's mechanical properties, but also resistivity without prejudice to magnetic properties. A couple of years later, silicon steel was massively produced in industry. In addition, silicon improves the resistance to corrosion and elastic limit of iron. All together, Fe-Si is probably the best alloy for low

frequency AC applications from magnetic, mechanical and economic points of view since its is composed only of cheap and abundant elements.

The silicon content can be varied in a very large range and forms BCC solid solutions up to 25 at.% Si, limit above which the alloys decompose into soft Fe_3Si soft phase and a Fe_7Si_3 hexagonal hard magnetic phase. Fig.1.8 shows the main properties of Fe-Si alloys. By increasing the silicon mass content up to 10%, the resistivity is multiplied by a factor 10 and the magnetization is reduced by 30% . However, the increase of the hardness makes the material very brittle above 10 at.% (5 mass%). This increase in hardness also makes the rolling more difficult and reduces life time of cutting tools. So, in practice (except the case of 6.5 mass%) Si content is usually between 2 and 4 mass%. For low-end applications (household and cars), low Si alloys are preferred to reduce the rolling and cutting costs. In contrast, for permanently plugged systems (network transformers, big generators) higher Si alloys with lower losses are preferred. Notice that most of Fe-Si alloys contains aluminium to help lamination. Usually, Al is less than 1 mass% and has effects on physical properties very similar to Si except for conductivity which is a little bit higher compared to equivalent amount of Si.

Processing

The mother alloys are produced from recycled silicon steels for a great part and pure iron (produced from iron ore) and silicon. The alloy is decarburized by blowing hydrogen in the melt and cast into a 20 cm by several meters slab. Then, it is reduced down to few mm by several hot rolling passes, followed by several cold-rolling passes depending on the silicon content and the final thickness. At this stage, the sheets are about 1 m wide in the form of a 1 m in diameter coil. The *semi-processed* materials are annealed at 800°C for a few minutes and rolled again with a small thickness reduction (skin pass). It is then sent to manufacturer for cutting and must be annealed in three steps: 750°C for decarburization under partial H_2 pressure, 800°C for grain growth and then in a wet atmosphere for surface insulation by oxidation. The *fully-processed* materials are annealed immediately after cold rolling at 800°C under partial H_2 pressure for decarburization, then up to 1000°C for grain growth and insulated by organic binder. The manufacturer can cut the sheets and mount them without further treatment.

Texture

Cold-rolling produces heavy deformation mainly by slipping in the most dense plane. In a BCC lattice, the most dense plane is {110}. Accordingly, successive cold-rolling pass tends to produce a {110} texture (grains have a {110} plane parallel with the sheet plane). However, cold-rolling is not perfectly anisotropic because all passes are made in the same direction, called rolling direction (RD). Consequently a slight anisotropy in the plane is observed corresponding to a small $\{110\}\langle 001\rangle$ texture and/or fibre type components

(mainly $\{111\}\langle 112\rangle$ see e.g. [35]). This kind of sheets are called non-oriented silicon steels (NOSS).

Because $\langle 001\rangle$ is the easy magnetization axis, permeability is stronger along RD compared to transverse direction (TD). Starting from this fact, metallurgists tried to improve the $\langle 001\rangle\{110\}$ texture in order to maximize the RD permeability. These materials are call grain oriented silicon steels (GOSS).

Designation of magnetic steels

There is no completely standard process for production of NOSS, if the general scheme described above is followed, each manufacturer has its own process and secrets. The result is that for the same grade, sheets from one provider or another could have slightly different texture and properties.

The grade of a magnetic silicon steels is defined by standards. The European designation for magnetic alloys follows the general one for steels that starts with a letter, here **M** for magnetic, followed by:

1. a number being hundred times total specific losses in watts per kilograms at a frequency of 50 Hz and an induction of:
   - 1,5 T for fully and semi processed NOSS and regular GOSS;
   - 1,7 T for low losses and high induction (Hi-B) GOSS;
2. a number corresponding to hundred times the thickness expressed in millimeters,
3. a letter corresponding to the type of silicon steel:
   A for fully-processed NOSS,
   D for non alloyed semi-processed steels,
   E for alloyed semi-processed steels,
   N regular GOSS,
   S low loss GOSS,
   P Hi-B GOSS.

For NOSS, standard thicknesses are 0.35; 0.5; 0.65 and 1 mm, but thinner gauge sheets (down to 100 μm) are more and more proposed by steel companies. GOSS are usually 0.35; 0.3; 0.27 et 0.23 mm thick, the two last being used generally for Hi-B.

Designation examples:

M 85-23 P Fe-Si grain-oriented sheet, 0.85 W/kg at 50 Hz under a 1.7 T sine waveform peak induction , 0.23 mm thick.

M 240-35 A Fe-Si fully-processed sheet, 2.4 W/kg at 50 Hz under a 1.5 T sine waveform peak induction, 0.35 mmm thick;

35 A 240 same in Japanese standard with permutation of numbers;

36 F 145 same in USA standard, with a small difference in thickness (due to older inch gauge) and 100×losses in W/lb at 60 Hz

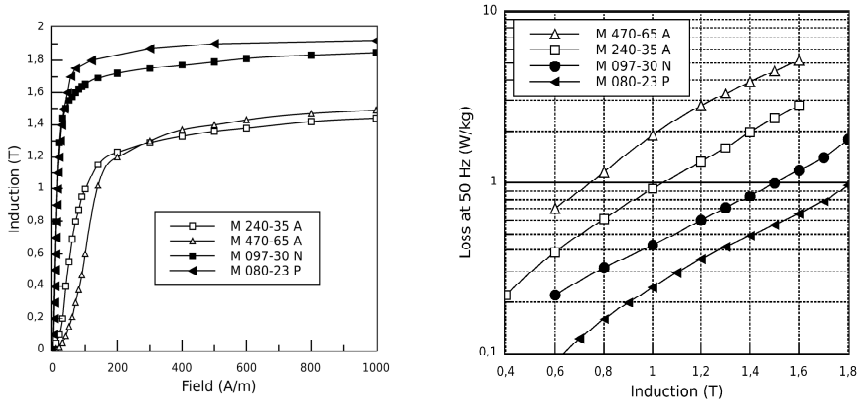

Fig. 1.9. Comparison of different common grades of oriented and non oriented Fe-Si sheets

1.3.2 Non oriented silicon steel sheets

NOSS are used in many different low frequency applications, because of their good mechanical and magnetic properties, in-plane isotropy and low price. They are proposed in a wide range of quality and price depending on the type of application and the requirements in terms of performances.

In general thicker gauges are cheaper, have higher losses and eventually better permeability. This is illustrated Fig. 1.9 where it is seen that thick gauge sheets have higher magnetization at low H and lower at high H (the cross point is here about 300-400 A/m) but the 50 Hz losses are always higher for thick gauges. As a consequence, they are used generally for low power household applications where price matters more than performance. In industrial applications, the power is usually higher and the cost of losses over the whole life of the device has to be taken into account in the economic balance. As the size of the device increases, heat is more difficult to release, so higher grade has to be used. If the working frequency is higher than the network frequency, thinner gauge can be used to reduce eddy current losses that becomes predominant above several hundred Hz. High grade NOSS are used essentially in industrial electrical machines where the flux is not everywhere parallel to lamination directions in stator teeth, and rotating in stator core.

The NOSS are considered isotropic in plane but this is not exactly observed in practice. At low field losses are almost independent of the direction of the field with respect to rolling direction (RD), though a little bit smaller at 0° as illustrated in the polar plot Fig.1.10. At 1.4 T losses are quite similar at 0 and 90° but they show a marked maximum around 45°. For this reason, according to the standard, losses have to be measured using strips cut in four different directions (0, 30, 60 and 90°).

Cutting

The fully processed sheets are delivered in the form of annealed and insulated sheets. The user cuts it in the required shape using punching, water jet or laser but losses are guaranteed only for Epstein format strips (300 mm × 30 mm). Because cutting always affects locally the magnetic properties, users have to keep in mind that losses could be higher in narrower zones such as stator teeth.

The semi-processed sheets have to be annealed after cutting. In this case, if the user anneals cut parts in the conditions given by the provider, losses are guaranteed in all parts whatever could be the cutting process or the size of cutting. However, this annealing has a cost for the user, so because semi-processed sheets are cheaper than fully-processed, many electrical machine manufacturers uses semi-processed sheets without annealing. In this case, properties are no longer guaranteed and can be significantly different from those claimed by the provider. Typical grades of semi-process silicon steel range between M-50-340-D and M-65-1000-D.

Thin gauge steels

In embedded power applications, in particular in electric vehicles, power density of electrical machines is the main issue after energy storage. For this purpose manufacturers increase the working frequency with a consequence on iron losses. This led metallurgists to develop low thickness NOSS. Fig.1.10 shows that reducing the thickness obviously lowers the eddy current losses, but increases the hysteresis loss. For the standard point, the lower losses are obtained for a thickness of about 0.25 mm. As the frequency increases above 400 Hz, advantage is clearly for the thinnest gauge.

An overview of NOSS properties is given in Table.1.1

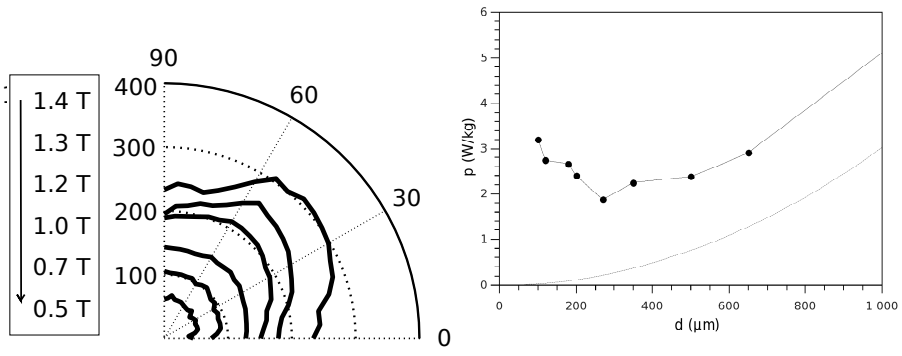

Fig. 1.10. Power loss as a function of fields angle with respect to rolling direction at 50 Hz,(left). Power loss at 1.5 T, 50 Hz as a function of thickness. Points are for higher grade material, line is for eddy currents (right)

Table 1.1. Magnetic properties of Fe-Si alloys fully process sheets . [27]

Reference	Si content (mass%)	ρ ($\mu\Omega$cm)	$B(T)$ @ 2.5 kA/m	H_Cé (A/m)	$p_{1.5}^{50}$ (W/kg)	$p_{1.5}^{400}$ é (W/kg)	$p_1^{2.5k}$ (W/kg)
M350-10-A	3.5	52	1.53		3.20	29.7	119
M270-20-A	3.5	52	1.59		2.4	29.7	205
M210-27-A	4.3	62	1.49	30	2.04	31.4	235
M235-35-A	4.1	59	1.53	35	2.25	41.2	249
M270-35-A	3.5	52	1.54	40	2.47	41.8	353
M330-35-A	2.7	42	1.56	40	2.94	57.9	517
M250-50-A	4.1	59	1.55	59	2.38	60.7	617
M400-50-A	2.7	42	1.59	50	3.57	91.7	899
M600-50-A	1.7	30	1.63	85	5.17		
M800-50-A	1.0	23	1.65	23	6.60		
M310-65-A	4.1	59	1.56	35	2.90		
M800-65-A	1.3	25	1.65	100	6.74		
M600-100-A	3.5	52	1.59	40	5.11		
M1000-100-A	1.7	30	1.65	85	8.89		

1.3.3 Grain oriented silicon steel sheets

By opposition to electrical machines for which the magnetic core should be isotropic, the ideal material for transformers should be anisotropic with easy axis corresponding to rolling direction (RD). Suitable texture should be either cubic $\{100\}\langle001\rangle$ or $\{110\}\langle001\rangle$. The second one is known as Goss texture from the name of its inventor, but coincidently, GOSS also means Grain Oriented Silicon Steel. For bcc cristals, the slip planes are highest density planes, $\{110\}$, so Goss texture is in principle easier to obtain. The advantage of using GOSS in applications where the flux is mainly directed along the easy axis is clearly illustrated in Fig.1.9, the induction at 800 A/m is almost 20% higher compared to NOSS and the loss at 1.5 T/50 Hz lower by a factor 4 to 10.

Conventional GOSS

Typical GOSS process starts by melting of an alloy containing about 3.2% silicon and 0.03% carbon followed by hot rolling down to 2 mm after heating to about 1300-1400°C. Then the sheet is annealed and cold rolled with a reduction rate of about 70%, annealed at 900°C and cold rolled again with a reduction rate of 50%. The coil is then decarburized in wet hydrogen and nitrogen at 800°C, coated by MgO, wound into a coil and finally annealed between 1100 and 1200°C in dry hydrogen. The MgO coating is necessary to avoid sticking of the turns during annealing and it reacts with Si to form an Fe-Mg silicate at the surface, a glass film also useful to ensure electrical insulation. The last thermal treatment produces the secondary recrystallization yielding the texture if a proper growth inhibitor (usually MnS) is used to impede primary recrystallization that would lead to isotropic texture. The conventional GOSS have much improved permeability and losses compared to

Table 1.2. Magnetic properties of grain oriented Fe-Si alloys. p_B^f is for the loss at induction$B$ and frequency f, B_H is the induction at field H expressed in A/m. [34]

Standards	ρ ($\mu\Omega$cm)	$p_{1.5}^{50}$ (W/kg)	$p_{1.7}^{50}$ (W/kg)	B_{800} (T)	$B_{2.5k}$ (T)
M075-23-N	49	0.70	1.00	1.76	1.92
M083-27-N	46	0.80	1.17	1.76	1.92
M090-30-N	46	0.87	1.24	1.74	1.91
M110-35-N	46	1.02	1.47	1.74	1.90
M090-20-S	49	0.61	0.88	1.80	1.93
M095-23-S	49	0.64	0.91	1.81	1.94
M110-27-S	46	0.74	1.03	1.81	1.94
M120-30-S	46	0.83	1.14	1.82	1.94
M135-35-S	46	0.91	1.26	1.83	1.96
M090-23-P	48	0.63	0.87	1.89	1.97
M095-27-P	48	0.69	0.93	1.90	1.98
M100-30-P	48	0.74	0.99	1.90	1.98
M115-35-P	48	0.87	1.14	1.90	1.98

NOSS if the field is applied in the RD, but it is degraded when the field is applied perpendicularly. As a consequence, transformer cores should be preferably built from straight parts rather than from EI cuttings (see Fig.1.12 in such a way the flux is always parallel to RD.

High induction GOSS (HiB)

HiB sheets are manufactured using a process very similar to the conventional GOSS except that cold rolling is realized in one pass only with almost 85% reduction and that AlN is added to MnS as growth inhibitor. The result is an anomalous grain growth of $\{110\}\langle 001\rangle$ crystals that can become very big (several cm). The magnetic domains are also very big which produces large excess loss according to Pry & Bean [29]. A common method to reduce dynamic losses is laser scratching. It consist in making laser spot lines transversely to the RD (more or less one spot each 0.1 mm and one line each 5 mm) that act as domain pinning points reducing their extension to about 1 by 5 mm. In addition more sophisticated glass films have been developed with low dilatation coefficient – at least twice smaller than that of Fe-Si ($12 \cdot 10^{-6}\mathrm{K}^{-1}$). During annealing, internal stresses are released, but after cooling the sheets remains under the tension of the glass film. Because of the positive magnetostriction of Fe-Si, the domains tends to be thinner and better oriented towards the RD and lancet domains due to out of plane disorientation are suppressed (see Fig.1.11).

Cutting

Conventional and HiB GOSS are mostly used in network frequency transformers. So in most of cases they work at 50 or 60 Hz at high induction over

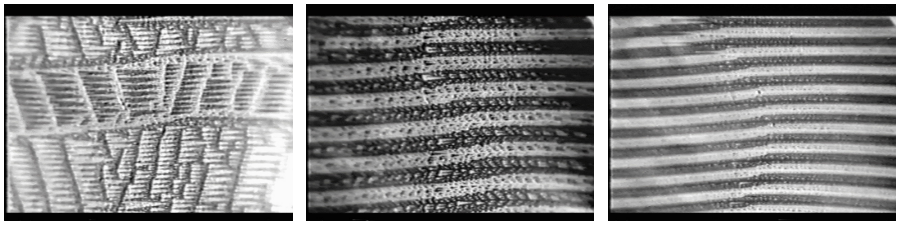

Fig. 1.11. Effect of tensile stress along rolling direction (horizontal) on the domain structure . From left to right, 4 MPa, 12 MPa, 24 MPa (courtesy of R. Barrué). Images are obtained by magneto-optical Kerr effect microscopy, see chap. MRI
.

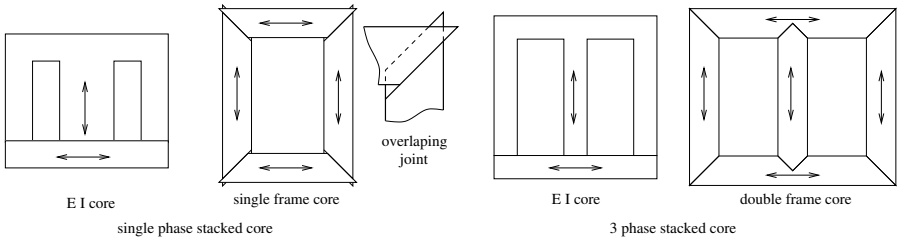

Fig. 1.12. Different types of stacked cores for transformers and inductors

1.5 T for conventional and over 1.7 T for HiB. The simplest way to built a transformer core is to stack sheets cut in E and I shape (Fig.1.12). The I is cut to make 2 windows in 2 face-to-face E. EI core are easy to realize: two stacks are made alternatively with E and I (or several E/several I), the coils made separately are sliped in one stack and the other is slotted in. EI cores have two disadvantages, the flux is perpendicular to RD in the yoke of the E and for 3-phase types, the window is bigger than the I so there is always a waste. If low loss and low EMI is required, strip wound cores are sometime used in the ring or rectangular form. The single or double frame cores are used for transformers above 1 kVA apparent power because the flux is mostly parallel to RD except at the corners. To reduce further the losses, the joints are cut at 45˚and overlapped.

Different type of cuttings and grades are used depending on the power of the transformer:

- $S < 1$ kVA, EI core cut in conventional GOSS (low added value products);
- $S < 1$ kVA, strip wound core from thin conventional GOSS (high added value products);
- $1 < S < 10$ kVA, frame core cut in conventional GOSS;
- $10 < S < 100$ kVA, frame core cut in low-loss GOSS;
- $S > 100$ kVA, frame core cut in HiB GOSS.

Table 1.3. Magnetic properties of 6.5% Si steels [24]. The resistivity is not given for graded materials since it is not constant.

Type	Thickness (mm)	ρ ($\mu\Omega$cm)	J_S @ 2.5 kA/m	$B(T)$ (A/m)	H_Cé (W/kg)	p_1^{50} (W/kg)	p_1^{400} é (W/kg)	p_1^{1k}
Graded	0.10	-	1.88	1.44	40	1.10	10.1	30.0
Graded	0.20	-	1.94	1.47	35	1.10	14.5	51.6
Uniform	0.05	82	1.80	1.38	26	0.70	6.50	18.8
Uniform	0.10	82	1.80	1.40	19	0.50	5.70	18.7

GOSS are also used for inductors either using EI cores with air gap (in this case layers are not alternated) or using cut strip wound rectangular cores. The latter, often called C cores are usually made from thin gauge (100 or 50 μm) and used in power electronics devices up to 10 kHz. In power plant generators, significant reduction of losses can be obtained using GOSS for the construction of the stator. Parts containing several teeth are cut and put with RD radial, whereas yoke parts are arranged with RD tangential.

1.3.4 Trends in Fe-Si products

Improved texture NOSS

The main drawback of {110} texture is related to the fact that this plane contains the ⟨111⟩ hard axes: when the magnetization turns from a ⟨100⟩ easy axis to another, it should pass through a ⟨110⟩ direction, but these axes are out of plane so a strong shape anisotropy is involved. The solution is to develop a {100} cubic texture , or at least to suppress a much as possible {111} components. For the same losses, the induction at $5\,\mathrm{kA}\cdot\mathrm{m}^{-3}$ is about 1.7 T, viz. 0.1 more than the best fully-processed materials.

Low Si alloys

Reduction of silicon content naturally leads to an improvement of the magnetization. For example reduction to 2% Si allows to reach 1.75 T at $5\,\mathrm{kA}\cdot\mathrm{m}^{-3}$ at the cost of higher losses (above 3 W/kg at standard point). These products are laminated with thickness between 0.5 and 1 mm for mechanical strength reasons. This larger thickness combined with lower resistivity results in an increase in eddy currents loss, so they are limited to network frequency use (Table 1.1). Due to their larger ductility, cutting cost is reduced but, because of larger magnetostriction, the properties are more dependent on the cutting technique and annealing conditions.

Silicon enriched electrical steels

Looking at the magnetic properties of Fe-Si alloys, it is seen that if saturation magnetization monotonically decreases, magneto-crystalline anisotropy and

Table 1.4. Main characteristics of Fe-Co alloys. Magnetostriction is given for isotropic alloys and ultimate strength σ_U is given for the hard state (for annealed state, divide by a factor 2 to 3).

Composition	form	t	density	T_C	ρ	J_S	λ_S	σ_U
		mm	kgm^{-3}	(°C)	$\mu\Omega$cm	T	10^{-6}	MPa
$Co_{49}Fe_{49}V_2$	strips, bars	0.1-1.5	8120	900	40	2.4	70	1200
$Co_{27}Fe_{73}Cr_{0.3}Mn_{0.5}$	strips, bars	0.1-3.5	8000	980	20	2.4	40	1000
$Co_{18}Fe_{79}Cr_3$	strips, bars	0.1-3.5	7900	940	30	2.3	30	850

magnetostriction do so as well and the latter is exactly zero for 6.5 w.% Si (12.14 at.%). As a consequence, this alloy has a large permeability, low loss and little sensitivity to stress. If its saturation magnetisation is lower than regular silicon steel, the induction under a field of 2.5 kA/m is comparable with GOSS. However, this alloy is very brittle and can't be laminated. A solution was found in the early 90's by Japanese company NKK (now JFE) introducing Si by chemical vapour deposition (CVD). Starting from a low Si laminated sheet, annealing in an atmosphere containing silane gas results in diffusion of Si into the metal. Using this method, the obtained material exhibits excellent mechanical and magnetic properties. 6.5 silicon steel sheets can be made with two different grades: uniform and graded Si diffusion. Because CVD is a diffusion process from the surface, the lamination is enriched at the surface only, then the silicon gradient can be controlled by the annealing time. Longer annealing leads to homogeneous diffusion in the bulk. The graded laminations have lower eddy current losses at high frequency because the eddy currents flow mainly at the surface. In contrast, they have higher hysteresis loss because there is a gradient of permeability and saturation magnetization across the thickness (see Table1.3.) Thus the choice of homogeneous or graded material depends essentially on the working frequency.

1.4 Iron-cobalt alloys

As shown by Pierre Weiss in 1912, alloying cobalt to iron has a spectacular effect on magnetic properties since Fe-Co has larger magnetization than iron. This is due to a modification of iron band structure, where the Fermi level is increased in such a way that 3d-up sub-band is filled by electrons from 3d-down sub-band (see chapter MMA).

Equiatomic Fe-Co alloy

Fe_2Co has the strongest room temperature magnetization known, but is relatively hard. However, the equiatomic alloy, known as Permindur, has a small anisotropy constant, a very soft behaviour, and still a very high room temperature magnetization, the reasons why it is preferred in spite of larger cobalt

Table 1.5. Magnetic properties of Fe-Co alloys of 0.35 mm thick strips

Composition	Annealing	B(800 A/m)	B(8 kA/m)	H_C	$p_{1.5}^{50}$	p_2^{50}	$p_{1.5}^{400}$	p_2^{400}
	°C	T	T	A/m	W/kg	W/kg	W/kg	W/kg
$Co_{49}Fe_{49}V_2$	750	2.05	2.28	120	3	5	44	84
	850	2.1	2.28	70	2.3	3.8	42	74
$Co_{25}Fe_{73}Cr_2$	750	1.47	2.02	200	6	9.5	70	140
	850	1.47	2.02	100				
$Co_{18}Fe_{79}Cr_3$	700	>1.7	<2	150	5.5	6.7	77	99
	900	>1.7	<2	260	3.3	4.3	66	88

content and higher cost (Table 1.4). In some applications, performance is more important than price of the elements. In airborne systems, the weight of a equipment is paid by fuel consumption at each take-off and power of the turbine needed to provide potential energy at 10 000 m from the ground. Under these condition a gain of 20% in induction results in a weight diminution of 20 to 30% and becomes economically favourable. FeCo has four big drawbacks: a low resistivity (below 10 Ωm), a brittleness that make rolling very difficult, a bcc to fcc phase transformation about 1000°C and an ordering near 730°C detrimental to magnetic properties and making the alloy even more brittle. Among all possible substitutions, 2% vanadium notably improves the resistivity, the ductility and the stability, but high temperature purification annealing is still impossible.

$Fe_{49}Co_{49}V_2$ is hot rolled down to about 2 mm, then heated and quenched in water to avoid ordering and finally cold rolled to a gauge between 0.35 and 0.1 mm. In this form, it is essentially used for transformers and the rotor/stator of airborne electrical machines, but it is also used in the bulk form for magnet pole pieces and electromagnetic valves for car thermal engines. The DC coercive force is relatively high compared to GOSS (see Table 1.5), but induction as high as 2.2 T can be reached in a field of less than 10 kA/m and works at 400 Hz with an induction of 2 T. Due to the large magnetostriction it must be annealed to release stresses at low temperature. Typically annealing just below the ordering temperature (750°) leads to anisotropic magnetic properties adapted for electrical rotating machines. Annealing at higher temperature (850°) reduces appreciably the losses but leads to ordering in a texture detrimental to machines but favourable for use as transformer cores. Its large magnetostriction (70 ppm) allows to use it as transducer or sensor in the lower acoustic band.

In addition to the high magnetization, Fe-Co is also interesting for its high mechanical strength. Indeed, in the near future, airborne generators are supposed to turn at 15-30 000 rpm for a power of 150-200 kW, so centrifugal forces acting on the rotor sheets will be critically high.

Table 1.6. Composition and structural properties of Fe-Co and Fe-Ni alloys

reference	Composition	form	t (mm)	density	T_C (°C)	ρ $\mu\Omega$cm	CTE (ppm/K)
Invar	$Ni_{36}Si_{0.25}Mn_{0.25}Fe_{63.5}$	strip, bars	0.5-10	8130	230	80	1
Mumetal	$Ni_{77}Fe_{14}Cu_5Mo_4$	strip, sheet	0.1-4	8700	400	60	12
Mo5-Permalloy	$Ni_{80}Fe_{15}Mo_5$	strip, sheet	0.1-1	8700	420	60	12
Mo6-Permalloy	$Ni_{81}Fe_{13}Mo_6$	strip, sheet	0.1-1	8700	420	60	12
36Fe-Ni	$Ni_{36}Fe_{64}$	strip, sheet	0.1-0.35	8100	230	75	1
40Fe-Ni	$Ni_{41}Fe_{59}$	strip, sheet	0.1-0.35	8150	330	60	4.5
50Fe-Ni	$Ni_{48}Fe_{52}$	strip, sheet	0.08-0.35	8200	450	60	8
Thermalloy	$Ni_{50}Fe_{41}Cr_9$	strip, disc	>0.4	8200	260	100	10
Thermalloy	$Ni_{50}Fe_{40}Cr_{10}$	strip, disc	>0.4	8200	230	100	10
Thermalloy	$Ni_{30}Fe_{65}Cr_2Cu_3$	strip, disc	>0.4	8150	120	88	6.6
Thermalloy	$Ni_{30}Fe_{65}Cr_2Cu_3$	strip, disc	>0.4	8100	55	80	1

Low cobalt alloys

Because of the price of cobalt, users always try to reduce the cobalt content. Typical low-cobalt alloys contain about 25 or 18 %, to ensure saturation far above iron one (i.e. 2.2 T). This is however paid by an increase in coercivity and losses as shown in Table 1.5. These alloys have lesser performance compared to equiatomic ones, but can be used advantageously in several cases, for example in landing gear motors which work only several seconds per flight (so losses have no relevance) or in airborne transformers because of the smaller magnetostriction producing less noise. Today's tendency is to improve the texture of low-Co alloys (easy axis parallel RD) for transformer applications in order to reduce loss and effective magnetostriction.

1.5 Iron-nickel alloys

Iron-nickel alloys were studied for the first time by Hopkinson in the 1890's and by others later for fundamental studies —and in particular by Guillaume who discovered Invar—, but it was only by the 1910's that Elmen from Bell labs obtained Fe-Ni alloys with permeability greater than that of pure iron. Invar is not properly speaking a soft magnetic material as it is used only as a zero thermal expansion coefficient (CTE) material. It is quoted here for historical reasons and because this feature is due to compensation of thermal expansion and volume magnetostriction around room temperature (above T_C Invar has thermal expansion comparable to other metals). Besides Invar, Fe-Ni alloys are of two kinds: bcc Fe-Ni (less than 30% Ni)and fcc Fe-Ni (more than 30%). In general there are no applications for the bcc form since they do not exhibit better properties than Fe-Si at a higher price. By contrast, the fcc form has many applications because a great variation in J_S, μ_R, H_C, T_C is observed with the Ni content. The most striking figure of these alloys is the

strong dependence of magnetocrystalline anisotropy on order. Indeed, when slowly cooled after annealing in the range of 900-1200°C, the alloy is ordered and $K_1 = 0$ for 56% of Ni. In contrast quenched alloys have $K_1 = 0$ for 73% of Ni. As a consequence, Ni rich alloys are usually quenched and the Fe rich ones slowly cooled.

More details on the fundamental aspects of Fe-Ni alloys magnetism can be found in chap. MMA An overview of industrial Fe-Ni soft magnetic alloys is given in Table1.6, they can be classified into three main families described below.

Table 1.7. Magnetic properties of Fe-Ni alloys. Py is the usual abbreviation for Permalloy, R and F are for rectangular and flat hysteresis loops respectively.

Reference	J_S (T)	H_C (A/m)	μ_i	μ_{max}	B_R/J_S	Loss (W/kg)	λ_S(ppm)
		static	static	static	%	p_B^f	
Mumetal	0.78	1.6	40	110		$p_{0.5}^{50} = 0.04$	
Mo5-Py	0.80	0.8	75	200	50	$p_{0.5}^{50} = 0.02$	1
Mo5-Py R	0.80	0.8	75	200	85		1
Mo5-Py F	0.80	0.7	100	130	20		1
Mo6-Py	0.66	0.4	300	130	50		0
36Fe-Ni R	1.30	15	3	20		$p_1^{50} = 1.1$	20
36Fe-Ni	1.30	55	2	7			
40Fe-Ni	1.45	6		66			
50Fe-Ni	1.60	8	4	35	50	$p_1^{50} = 0.1$	24
50Fe-Ni R	1.60	9		100	95		
50Fe-Ni F	1.60	1.5	40	100	30		

1.5.1 Ni-rich alloys

These alloys are currently called permalloy after Elmen from Bell labs in 1920 and their composition is always close to 80% Ni, for this composition the material undergoes a spin reorientation transition (say a change of easy axis from [111] to [110]) around room temperature and zero magnetostriction together in the disordered state. For this reason, the material properties are very sensitive to the microstructure and order, so the heat treatment can change drastically the magnetic characteristics such as coercivity and permeability. Typical heat treatment consists in heating over 1000°C , then cooling to 600°C and quenching in air. This procedure retains disorder and promotes high permeability for $Ni_{75}Fe_{25}$. Alternatively long-time annealing followed by slow cooling (1 day) produce recristallization and forms a Ni_3Fe-like ordered alloy. In this case the maximum permeability is obtained for lower Ni content. The drawback of Fe-Ni alloys is the relatively low resistivity because the two elements are from the iron group and have similar electronegativity. In industrial permalloys, 4 to 6% molybdenum is usually added to increase the

resistivity and to ensure minimum magnetocrystalline anisotropy and magnetostriction. For example, 5% Mo substituted to Fe in $Ni_{80}Fe_{20}$ results in a increase in resistivity from 20 to 60 $\cdot 10^{-8}$ Ωm, but at the same time, saturation magnetization is decreased from 1.05 to 0.8 T. Typical Mo-Permalloy contains 5% Mo and 80% Ni, and the magnetic properties can be changed by the heat treatment: quenched, slowly cooled, recrystallized or annealed in field. Annealing is conducted in pure dry hydrogen usually between 1000°C and 1200°C to remove impurities (C, O, S...). The permeability can be enhanced by increasing treatment temperature (less impurities, bigger grains). Rectangular hysteresis loop are obtained by slow cooling promoting ordering. For this composition, the easy axis becomes [111] which (due to the six-fold symetry) leads, in theory, to a remanence ratio of 87% , very close to the experimental value. By opposition, flat loops are obtained by annealing under a magnetic field applied perpendicular to the strip. A first annealing is conducted at low temperature (about 500°) to adjust $K_1 = 0$ and followed by field annealing below T_C. Mo5 Py, is used in any application where very high permeability and very low coercivity are necessary if magnetization is not a dimensioning parameter (typically ground fault detector, current transformer). Rings (toroids) realized by strip winding is the most used shape for Permalloy, but strip wound rectangular cut cores are often used for inductors. In applications where both $K_1 = 0$ and $\lambda_s = 0$ are required (typically for flexible magnetic shields) the composition is modified to 6% Mo and 81% Ni. If higher Curie point and magnetization are required, 4% Mo 80% Ni alloy is preferred.

Mumetal is a variant of permalloy in which several % of copper are added to improve the ductility. This reduces the cost of both lamination and forming processes, so it is used generally for large rigid magnetic shields or zero field chambers.

1.5.2 Fe-rich alloys

Iron rich alloys contain at least 30% of nickel, they always have the fcc structure. Equiatomic alloy is the most used because it offers a nice combination of high magnetization and permeability together with low coercivity and losses. However, this alloy exhibits relatively low resistivity which is detrimental to losses in high frequency applications (see Table 1.6). In this case, 36Fe-Ni may be used but T_C is decreased by 100 K as it is closer to the Invar composition. Iron-rich alloys can be processed by three routes.

1. Moderate hardening (60% skin pass) and 1100°C annealing under H_2 lead to isotropic texture. This treatment results in an isotropic magnetic behaviour and low losses. The permeability is moderate compared to Ni-rich alloys but much higher than NOSS. An induction of 1 T is obtained in a field of only 10 A/m, an order of magnitude lower than NOSS or FeCo. These features are ideal for small and efficient electrical machines, when

the power density is not a key issue. They are currently used in the form of stamped sheets for stators or rotors and in the form of bulk parts in electromagnetic relays.

2. Strong hardening (>90%) and > 1100°C annealing produce an anisotropic cubic texture $\{100\}\langle 001\rangle$, leading to very high rectangularity. Growth inhibitors (selected impurities) have to be added in the alloy to stabilize the texture and avoid secondary recrystallization which slightly increases the coercivity. They are suitable for low loss transformers, especially at 400 Hz or above, as the permeability is very high, and in applications where high rectangularity is needed such as magnetic amplifiers or different types of sensors (fluxgate, see chap. SEN).
3. Secondary recrystallization at high temperature (> 1100°C) of high purity alloy results in anomalous growth of crystals. Subsequent field annealing just below T_C produces uniaxial anisotropy in the direction of the applied field. 55Ni alloy is preferred because K_1 is appreciably smaller in the ordered state compared to alloy containing 48% of Ni. The field induced anisotropy is of order 400 Jm^{-3} which is a bit stronger than the magnetocrystalline one of the ordered alloy (about 200 Jm^{-3}) and sufficient to flatten the loop. The remanence to saturation is low, so the material demagnetizes itself: this feature associated to high induction is interesting for unipolar transformers (the maximum induction swing is $\Delta B \leqslant J_S - B_R$), or in any application similar to that of their Ni-rich counterparts (current transformers,energy meters, etc.) but with smaller price due to the smaller Ni content.

1.5.3 Thermal alloys

Thermal alloys have been originally developed to compensate the effect of thermal fluctuation in magnetic circuits. These alloys have usually a composition close to $Fe_{30}Ni_{70}$ which is at the limit between BCC and FCC phase and has a Curie point of 50°C. Cr is generally added in the composition since it moves the BCC/FCC limit to lower Ni content and offers a an additional parameter to control T_C together with a reduction the price of the elements.

This is particularly useful for permanent magnet circuits which are usually quite sensitive to temperature. When a highly-stable induction in the gap of a magnetic circuit containing a permanent magnet is required, a thermal alloy part is used as a shunt to the magnet. It was used in the past in electrical measurement instruments, tachometers, relays... but today most of these applications are obsolete. Recently a new class of applications appeared for controlled Curie point materials, i.e. induction cookware. In this application, a magnetic layer is needed to concentrate the flux in the pan bottom and maximize the energy transfer. Associated to the copper layer (needed to ensure thermal homogeneity and strong eddy currents) and the stainless steel pan body, the alloys must have a similar dilatation coefficient to the other

materials. Advantageously, the Curie point may be adapted to naturally regulate the temperature to avoid burning the food but also for safety as T_C can be tuned below the ignition point of oil. For frying pans, the Curie point is 260°C, whereas for other pans it can be lower (230°C) or only just above boiling point of water (120 °C). Eventually this natural regulation reduces the electrical stress on the inverter, limiting regulation switching.

1.6 Amorphous and nanocrystalline alloys

The amorphous state of matter, or glassy state, is a solid state having no long range order. In a first approach, amorphous solids are considered to have tetrahedral local order. An amorphous state of matter is natural for silicates formed by rapid cooling of lava to form obsidian or volcanic glass. However, only metallic glasses are magnetic and pure metals (or transition-metal alloys) cannot be obtained in the glassy state. Thus some elements called glass formers, must be added and the quenching rate must be of the order of magnitude of 10^6 K/s [1]. The glass former must have smaller atomic radius than transition metals and eventually, an addition of a bigger atom (refractory metal) can help. To be magnetic, a glass must contain more than 60% of transition metals carrying magnetic moment. The general formula is $T_{1-x-y}M_xR_y$ where for industrial material:

T = Fe, Co, Ni and 70>T>80 at.%;
M = Si, B and 20>M>30 at.%;
R = Mo, Nb and R<3 at.%.

At the industrial scale, the alloys are prepared from pure elements except boron provided by F_3B or F_2B compounds. The elements are usually melted by induction in vacuum and poured in a crucible maintained at a temperature several degree higher than the melting temperature (1100-1300°C). The liquid metal is projected by inert gas into a nozzle fitted with a thin slit very close to the rim of a cold wheel turning with a peripheral speed of about 30-40 m/s. This process is known as planar-flow casting. The rim is usually made of copper – or copper alloy, e.g. Be brass – to ensure efficient thermal transfer and water cooled. If the parameters, speed, pressure, temperature are properly tuned, the alloy is directly transformed into a ribbon having a width equal to that of the slit and a thickness of about 20 μm. Depending on the application, the thickness can be tuned between 18 and 40 μm and the width from several mm to over 100 mm.

The as-quenched ribbons are in the amorphous state but they have to be annealed to release quenching stresses and optimize the magnetic properties.

[1] Bulk metallic glasses have been successfully produced by the end of the 90's, but they have relatively low magnetization. In addition the bulk state is a drawback for applications, so they have never been produced at industrial scale

In the case of cobalt-based alloys, annealing also partly releases free volume. Because iron based alloys do not retain free volume, annealing results in a significant embrittlement. Annealing is usually at about 350-400° for cobalt-based and 400-450° for iron-based alloys.

1.6.1 Iron based amorphous alloys

The iron-based amorphous alloys exhibit the highest magnetization of all amorphous materials due to the large iron content, about 1.6 T (eventually, magnetization can be improved by cobalt addition up to 1.8 T). As a consequence, they are particularly fitted for low and medium frequencies when high magnetization is the first dimensioning parameter. Because of the long range disorder, the magnetocrystalline anisotropy is theoretically zero, but the magnetostriction is usually quite strong (about 25 ppm). This strong magnetostriction has been sometimes used for sensors or transducers, but in general it is detrimental to the magnetic properties because internal stresses cannot be totally released, so the permeability remains within the order of magnitude of 10^5 'only' and the coercive field is never below several A/m. In the 80's a large variety of iron-based amorphous alloys have been developed, in particular by Metglas:

A1, for low frequency applications and in particular network transformers;
S3, for high frequency power electronics;
SC, for magneto-elastic based applications (transducers and sensors);
CO, for same applications as SA1 but with higher induction.

Table 1.8. Composition and structural properties of metallic glasses and nanocrystalline ribbons [22, 23, 37]

reference	Composition	t (μm)	T_X (°C)	density	E (MPa)	α (ppm/K)
Metglas 2605A1	$Fe_{78}B_{13}Si_9$	25	550	7.18	<110	2.0
Metglas 2605S3	$Fe_{77}Cr_2B_{16}Si_5$	20	535	7.29	<110	6.7
Metglas 2605SC	$Fe_{81}B_{13.5}Si_{3.5}C_2$	20	480	7.32	<110	5.9
Metglas 2605CO	$Fe_{66}Co_{18}B_{15}Si_1$	25	430	7.56	<110	8.6
Metglas 2826MB	$Fe_{40}Ni_{38}Mo_4B_{18}$	20	410	7,90	<110	
Metglas 2714A	$Co_{66}Fe_4Ni_1B_{14}Si_{15}$	18	550	7,59	<110	
Metglas 2705M	$Co_{69}Fe_4Ni_1Si_{12}Mo_2B_{12}$	20	520	7.80	<110	
Vitrovac 6025	$Co_{66}Fe_4B_{12}Si_{16}Mo_2$	20	530	7.70	<150	
Vitrovac 6155	CoBSi	20	480	7,84	<150	
Vitrovac 6030	$Co_{70}(Fe, Mo)_2Mn_5(B, Si)_{23}$	20	480	7.60	<150	
Vitrovac 6006	$Ni, Co, Fe)_80(B, Si)_{20}$	20	430	7.80	<150	
Vitroperm 800	$Fe_{73.5}Si_{15.5}B_7Nb_3Cu_1$	20	630	7.35	190	
Vitroperm 500	$Fe_{74.5}Si_{13.5}B_8Nb_3Cu_1$	20	630	7.35	190	
Finemet	$Fe_{73.5}Si_{13.5}B_9Nb_3Cu_1$	18	630	7,40	180	

However, today only Metglas 2605SA1 is produced as iron based alloy. They are used essentially in network transformers. Compared to GOSS, they have much smaller working induction, but also much smaller losses Fig.1.13. Transformers made from amorphous cores are more expensive because of a larger amount of magnetic material required and more complicated construction, but as they save unload losses, they are economically viable considering the cost of losses integrated over 30 years life. Network transformers rating over 100 kVA are currently developing owing to the cost of energy. Most of them are 5 limbs type made from 4 rectangular rolled open frames. Properties of Metglas SA1 have not been improved significantly since the 80's, only recently Metglas has proposed a new alloy with improved induction (HB) obtained by using a larger amount of Fe (about 85 at.%) but still not available.

Iron based amorphous metals are used also in the form of C-cores cut from rolled rectangular frame or powder cores.

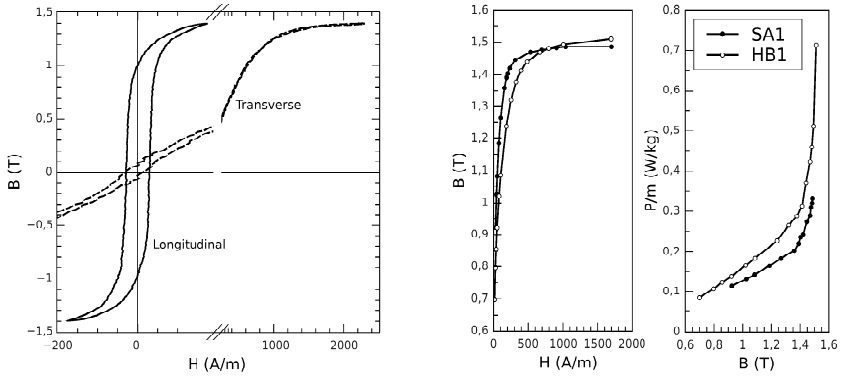

Fig. 1.13. Left: hysteresis loops of Fe-based Metglas SA1 samples annealed in longitudinal and transverse field. Right: comparison of magnetization and iron loss curves of Metglas SA1 and HB

1.6.2 Cobalt based amorphous alloys

Due to the smallest magnetic moment of cobalt atoms compared to iron, cobalt-based alloys have markedly lower magnetization than iron-based ones (see Table1.9. In contrast, because they have a very low magnetostriction and low internal stresses (as they retain free volume), they have the smallest coercivity of all magnetic materials known and the highest permeability. In addition, thanks to this nearly zero magnetocrystalline and magnetoelastic anisotropy, uniaxial anisotropy can be induced by field annealing resulting in perfectly square or perfectly linear hysteresis loop (Fig.1.6.1 left box). These features are particularly interesting for saturable cores or when both high

permeability and linearity are required. Because the cobalt is expensive, they are limited to high value added applications (sensors) or to applications where a small quantity of material is required (anti-theft tag).

1.6.3 Nanocrystalline alloys

Nanocrystalline alloys, known as Finemet (Hitachi trade mark) have been discovered in 1988 from iron-based amorphous alloys of specific composition [40]. The amorphous ribbon is produced by the same process as others, except that the annealing temperature is pushed to 530-550°C to partially devitrify the alloy. Copper forms very small clusters playing the role of nucleating agent for Fe-Si particles, whereas Nb acts as growth inhibitor. The result is an homogeneous distribution of 10-15 nm $Fe_{80}Si_{20}$ particles representing about 65 vol.% in the optimal state, embedded in the remaining amorphous matrix [33]. Owing to the small grain size, the anisotropy is averaged over the exchange length resulting in a nearly zero anisotropy following the mechanism proposed in [2] and demonstrated conclusively in nanocrystalline materials

Table 1.9. Magnetic properties of metallic glasses and nanocrystalline ribbons. M is for Metglas ([22]), VP for Vitroperm (Vacuumschmelze [37]), FT for Finemet (Hitachi [23]), NP for NanoPhy (Aperam [5])

Reference	J_S (T)	H_C (A/m) static	μ_{max} static	B_R/J_S %	Loss (W/kg) 100kHz, 0.2 T	T_C (°C)	ρ (Ωm)	λ_S(ppm)
M 2605A1-Z	1.56	2.4	40 000	90	500	415	1.3	27
M 2605A1-F	1.56	2.4	6000	5				
M 2605S3-A	1.41	4.8	35 000	50	90	358	1.38	20
M 2605SC	1.61	3.2	30 000		600	370	1.25	30
M 2605CO	1.8	4	25 000	4	90	145	1.23	35
V 6006	0.42		500	95		150	120	
M 2826MB-Z	0.88	0,4	80 000	90	500	353	1,38	12
M 2826MB-F			30 000	5				
M 2714A	0.55	0,3	115 000	95	50	205	1,42	$\simeq$0
M 2714A	0.55	0,3	30 000	95	45	205	1,42	$\simeq$0
M 2705M	0.77	1.2	600	*	100	365	136	$<$1
V 6025-Z	0.55	0.3	1000	95	50	210	140	0,2
V 6025-F			100 000	5				
V 6155-F	1	0,8	1000	5	58	485	110	
V 6030-Z	0.82	1	300 000	95	80	365	130	0.2
V 6030-F			3500	5				
VP 800-F	1.2	0.5	100 000	8	40	600	1.15	0,5
VP 500-F	1.25	0.5	20 000	4	40	600	1.15	0,5
FT-3H	1.23	0.6	30 000	89	80	580	1.35	2,3
FT-3M	1.23	2.5	70 000	50	40	580	1.35	2,3
FT-3L	1.23	0.6	17 000	5	34	580	1.35	2,3
FT-3M	1.23	2.5	70 000	40	40	580	1.35	2,3
NP Kμ	1.27	$\simeq$6	200-3000	1	100	580	1.35	$<$1

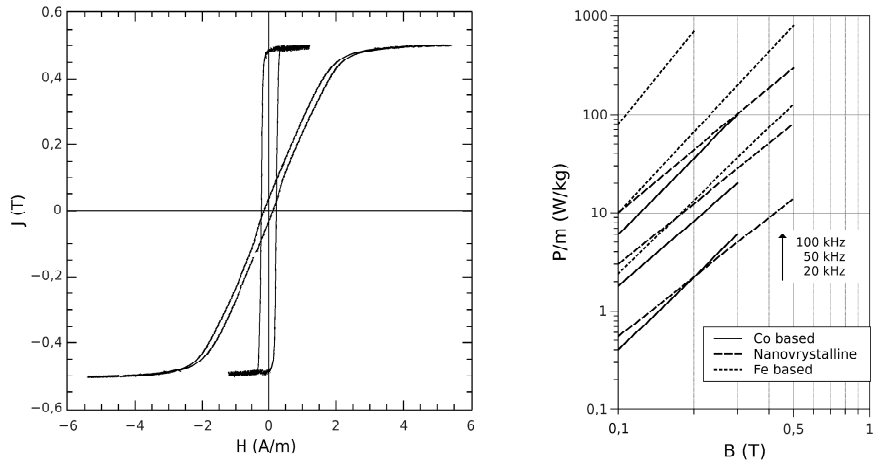

Fig. 1.14. Hysteresis loops of longitudinal and transverse field annealed cobalt-based amorphous alloy (V6025). Left, iron loss as function of induction for various frequencies in Co-based Metglas 2714, Finemet and and Fe-based Metglas SA.

by Herzer [20]. In addition, because the $Fe_{80}Si_{20}$ nanocrystals have negative magnetostriction whereas the amorphous remaining phase (composition close to $Fe_{70}B_{30}$) has a positive one, proper tuning of the Si content and the annealing leads to compensation down to nearly zero [21]. As a consequence, Finemet type nanocrystalline materials have advantages of both iron-based and cobalt-based amorphous, namely, high magnetization and extreme softness. As cobalt-based metallic glasses, longitudinal field annealing produces squares loops and transverse field annealing flat loops with high linearity and low squareness (Fig. 1.15 left box). Compared to amorphous alloys, Finemet exhibits loss much lower than Fe-based alloys and equal to Co-based at lower price and possibly higher induction (Fig.1.6.1 right box).

The most striking figure of this alloys is the effect of stress applied during annealing. As shown firstly by Glaser [19], stress annealing induces a very strong anisotropy perpendicular to the tension direction and directly proportional to the tension applied. This results in very flat and linear loops those permeability can be directly controlled by the stress according to $\mu_R \simeq 7 \times 10^4/\sigma$ where the stress σ is expressed in MPa [3]. Stress annealed strips are currently produced using Arcelor-CNRS process [4] and usually rolled into ring shape. These components have the capacity to store energy, not in an air gap as usual but in the material itself. The advantage of stress annealed nanocrystalline cores compared to gaped-core or powder cores is a much higher linearity, lower losses for same energy stored and absence of flux leakage. Among all soft magnetic materials, Finemet type nanocrystalline alloy is from far the most versatile since its permeability can be tuned from 200 to 100 000 depending on the field or stress applied during the nano-

crystallization heat treatment (Fig. 1.15 right box). As a consequence, they can be utilized in a wide range of applications where a high permeability is required with a flat or square loop as sensors, filters and transformers, where a low permeability and high linearity is required as chokes, inductors, sensors, filters etc.

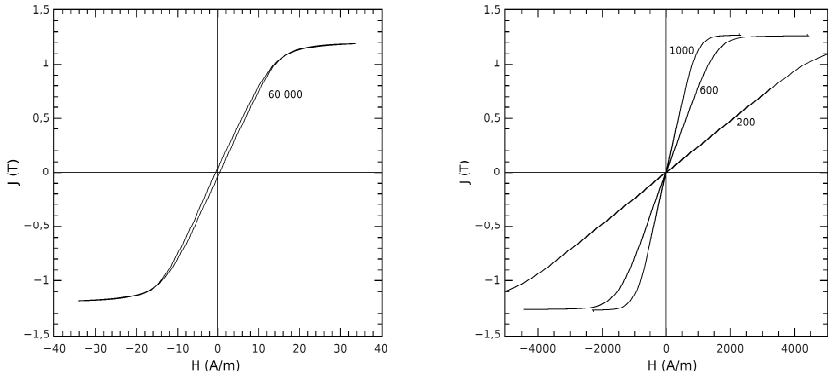

Fig. 1.15. Hysteresis loops of Finemet type nanocrystalline alloys (labels indicates permeability). Left transverse field annealed material from Vacuumschmelze, right, stress annealed samples from Aperam (Kμ). Note the two order of magnitude on x scale.

1.7 Soft ferrites

1.7.1 Spinnel ferrites

Spinel ferrites are iron oxides having the crystal structure of the mineral $MgAl_2 04$. The general formula of ferrites is $MFe_2 0_4$ where M is a divalent metal or a combination having a ionic radius compatible with available octahedral (B) and tetrahedral (A) sites of the lattice. Depending of the ionic diameter of the divalent metal, the spinel can be normal (divalent metal in A site, like Zn) or inverse (divalent metal in B site, like Fe, Co, Ni) or sometimes mixed (like Mn or combination of two divalent ions or even a combination of univalent and trivalent ions). Actually the position of M^{2+} depends both on its diameter (big ion goes in bigger B site) and electrostatic interactions (more charged ion goes in the B site). Because all magnetic exchange interactions are antiferromagnetic, the energy of the lattice is usually minimized for the minimum magnetic moment. Consequently, because Fe^{3+} has the largest magnetic moment (5 μ_B), Fe^{3+} moments cancel. In simple ferrites (when M is one element) the net magnetic moment per formula is given by that of M^{2+}.

The situation is a little bit more complicated for mixed ferrites, but very interesting when M is a combination of Zn and another ion holding a magnetic moment. Because Zn goes in (A) and because it has a zero magnetic moment, the moment associated to (A) is reduced and if Zn content is smaller than 0.5, the magnetic order keep that of the inverse spinel so the net moment increases (see Table 1.10). This is often used in commercial ferrites in the aim of enhancing the magnetization. However, increasing the Zn content over 0.5 yields partial normal spinel magnetic order and thus a reduction of the magnetization. The reader would find more details in chapter MOX.

In spite of a strong magnetic moment, iron ferrite —aka magnetite, load stone— is not used as a soft magnetic material because of its relatively high coercivity. Fe^{2+} has a non zero orbital moment that leads to strong spin-orbit coupling and consequently strong spin-lattice coupling (in other words magneto-crystalline anisotropy). Another drawback of magnetite is its conductivity. Indeed, the Fe^{2+} is the octahedral site, which is favourable from ionic diameter point of view but unfavourable from electrostatic point of view, so hoping of an electron from Fe^{2+} to A site Fe^{3+} yield little change in energy and this hopping is made easier by thermal excitation. As consequence, magnetite is an intrinsic semiconductor, its conductivity is typically $10^{-4}\Omega$m at room temperature. It is thus important for high frequency application to replace totally all ferrous ions. Technically speaking, hundred kind of ferrites can be (and have been) made since elements from Ti to Zn plus Mg, Li, Al etc. can be substituted. Fortunately, Darwin's theory also applies to technology so few families only of ferrite have markets, mainly Mn-Zn and Ni-Zn and, in a much smaller extend Li and Mg ferrites.

1.7.2 Synthesis of sintered ferrites

Raw materials — Industrial ferrites are produced the ceramic route. In general the precursor materials are simple oxides: Fe_2O_3, MnO, ZnO, NiO, CuO, CoO... The purity and the grain size of the powders have significant influence on the final properties. Ideally, they should be fine and homogenous in grain size to ensure the chemical homogeneity.

Milling — After weighting the oxides as a function of the expected composition, the powder is milled in order to get an homogeneous mix with finer

Table 1.10. Distribution of ions in spinel sites for simple ferrites and example of a mixed ferrite

normal			inverse			$Zn_{0.25}Ni_{0.75}Fe_2O_4$		
(A)	$[B]$		(A)	$[B]$		(A)	$[B]$	
(M^{2+})	$[Fe_2^{3+}]$	O_4	(Fe^{3+})	$[Fe^{3+}M^{2+}]$	O_4	$(Zn\,3Fe^{3+})$	$[5Fe^{3+}\,3Ni^{2+}]$	O_{16}
tetra	octa		tetra	octa		tetra	octa	
$\uparrow$	$\uparrow\downarrow$		$\downarrow$	$\uparrow\ \uparrow$		$\cdot\downarrow\downarrow\downarrow$	$\uparrow\uparrow\uparrow\uparrow\uparrow\ \uparrow\uparrow\uparrow$	

grains. This operation is important to optimize the reaction. Usually the mill is made from stainless steel so excess iron may be brought at this stage.

Firing — The mix is heated in air at a temperature between 900 and 1100°C, depending on the grain size, to produce the solid state reaction. At this stage the spinel phase is formed.

Milling — Because firing produces grain growth, a second milling is necessary to refine the grains, preferably below 1 μm, before sintering. At this stage different additives can be introduced in small quantities such as V_20_5, to reduce sintering temperature, $Si0_2$, to limit grain growth, CaO, to increase the resistivity, etc.

Forming — The powder is now mixed with an organic binder (usually PVA) and pressed in a mould to give the final shape of the core. There is a great variety of shapes that can me made industrially: rings, E, I, U, pots, rods, screws, plates, tubes... Pressing is generally uniaxial, isostatic pressing is used only at laboratory scale to realize big cores or with complex shapes.

Sintering — To densify the core and to obtain good properties, sintering must be conducted with caution. Depending on the composition, the grain size before sintering and the expected grain size after, the temperature is usually above 900°C and up 1350°C. Sintering takes several hours and cooling rate must be low, particularly for bigger cores, in order to avoid cracking. NiZn ferrites are sintered in air, but MnZn ones must be sintered in controlled atmosphere. Indeed, the partial oxigen pressure in air is such that it would oxidize Mn^{2+}, so it must be controlled according to $\ln p_{0_2} = -K/T$.

1.7.3 Mn-Zn ferrites

Manganese simple ferrite is a mixed type one: Mn ions are found in both sites. Mn^{2+} substitution is very interesting because this ion exhibits a strong spin (5/2) and a zero orbital moment. Thus Mn based ferrites can be extremely soft.

Influence of chemical composition on intrinsic magnetic properties

The magnetic properties can be easily modulated by tuning the Mn to Zn ratio. Zn substitution has three main effects on properties:

- enhances the magnetic moment (within the limit of 0.5 per f.u.) as said before,
- affects AB exchange coupling resulting in a decrease in Curie temperature (T_C),
- reduces the magneto-crystalline anisotropy (K_1), thus tends to increase the permeability (μ_R).

Interestingly, because higher magnetic moment can be obtained only at the price of a reduction in Curie temperature, the highest magnetization at room temperature is obtained for a relatively small Zn content ($x \simeq 0.15$).

Mn ferrite has a low magnetocrystalline anisotropy (due to $3d^5$ configuration of ions) with a [111] easy axis, whereas Fe ferrite has strong anisotropy (due to Fe^{2+}) with a [110] easy axis. As a consequence, a controlled excess of Fe can produce a spin reorientation transition (SRT) revealed by a maximum in permeability and the SRT temperature will depend on the Fe^{2+} rate (usually less than 0.1). Fine tuning of this rate can maximize permeability at working temperature or making it stable on a wide range of temperature. Fig.1.16 is showing a typical thermal dependance of the permeability of a MnZn ferrite. Here the Zn and Fe^{2+} rate are tuned to get a SRT at 100°C as revealed by the second Hopkinson peak.

Thus choosing the composition of a MnZn ferrite is a compromise depending on the most dimensioning parameter of the application. Typical examples are given in Table 1.11.

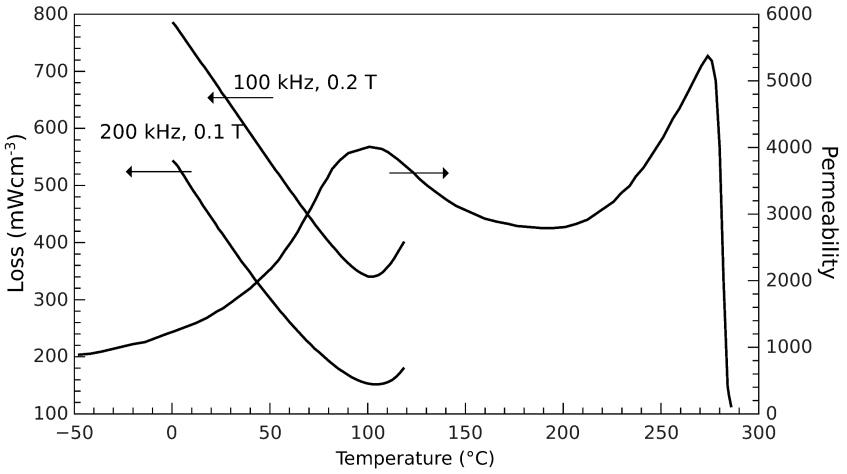

Fig. 1.16. Permeability and loss dependence of high frequency MnZn power ferrite

Table 1.11. Main applications of $Mn_{1-x}Zn_xFe_20_4$ and typical compromise on Zn content

Application	Main parameter	Zn content	T_C (°C)	M_S (T) 0 K	M_S (T) 300 K
Telecom transformers	M_S	0.2	250	0.7	0.54
Power transformers	T_C, M_S	0.3	230	0.78	0.5
Wide-band transformers	μ_R, T_C, loss	0.5	150	0.9	0.4
Signal transformers	μ_R	0.55	130	1	0.39

Influence of microstructure on extrinsic magnetic properties

The permeability, coercivity (H_C) or losses are micro-structure dependent properties. When the permeabilty is related mostly to domain wall motion, it is usually accepted as a first approach that:

$$\mu_R \propto \frac{1}{H_C} \propto \frac{J_S D}{\sqrt{K_1}} \tag{1.47}$$

where D is the grain size. So getting the highest permeability means large Zn content and coarse grains. However, MnZn ferrite, like magnetite have a relatively low resistivity (even without ferrous ions) due to electron hoping between divalent and trivalent Mn ions. The intrinsic resistivity of MnZn ferrite is about 0.1 Ωm so in high frequency applications eddy currents in the core would produce high losses (see 1.1.2). CaO is added for this purpose because it's an electrical insulator and because the ionic radius of Ca^{2+} is too big to enter in the spinel lattice. Thus after sintering CaO segregates at grain boundaries forming an insulating barrier of thickness t. The electrical resistivity can be written in a first approximation $\rho_{eff}(t+D) = \rho_{CaO}t + \rho_{MnZn}D$. As $\rho_{CaO}t \gg \rho_{MnZn}D$ and t and D are several nm and μm respectively:

$$\rho_{eff} \simeq \frac{t}{D}\rho_{CaO} \tag{1.48}$$

On the over hand, this insulating layer is paramagnetic, so the permeability is reduced by the air gap:

$$\mu_{eff} = \frac{\mu_R}{1 + \mu_R \frac{t}{D}} \tag{1.49}$$

As a consequence, in MnZn ferrites the increase in resistivity is always payed by a drop in permeability. A side effect of the CaO barrier, is grain growth and densification inhibition resulting in larger porosity. As a first approximation, if the material is porous, the factor $\frac{t}{D}$ in (1.49) is change for

Table 1.12. Main $Mn_{1-x}Zn_xFe_20_4$ materials used for broadband transformers, pulse transformers, common mode chokes, delay lines. References starting with a letter are from TDK, with a number from Ferroxcube.

ref.	x (approx)	B_{1k} (T) 25°C	B_{1k} (T) 100°C	μ_i ± 30%	f_R (Hz)	H_C(A/m) 25°C	T_C (°C)	ρ (Ωm)	f_{max}(Hz)
T46	0.55	0.40	0.24	15000	400 k	7	130	0.01	100 k
T38	0.55	0.43	0.26	10000	300 k	8	130	0.1	100 k
T36	0.55	0.40	0.24	7000	300 k	22	130	0.2	100 k
T37	0.55	0.38	0.24	6500	700 k	9	130	0.2	300 k
N30	0.55	0.38	0.24	4300	1 M	12	130	0.5	400 k
3E6	0.55	0.39	0.22	12000	400 k	5	130	0.1	100 k
3E7	0.55	0.39	0.22	15000	250 k	4.5	130	0.1	100 k

$\frac{t}{D} + d^{-\frac{1}{3}} - 1$ where d is the relative density. As a consequence, CaO alone reduces strongly the permeability. This effect is usually counterbalanced by addition of a flux. A flux is an oxide having a melting point lower than the sintering temperature: the liquid phase enhances strongly the diffusion and in turn favours the grain growth and density. For this purpose, SiO_2 and V_2O_5 are mostly used (by less than 1% of the mass), but everything depends on the customs of the manufacturer. In Table 1.12, properties of ferrites for broadband transformers typical application are presented. They have approximately the same Mn/Zn ratio, and a very good correlation is found between resistivity and permeability using (1.49) and (1.48). A typical example of permeability and loss dependance on temperature is given in Fig.1.16. Because high frequency power applications require low loss, the insulation layer must be thick enough. To compensate the decrease in permeability, the SRT is tune to get a high permeability at the working temperature (here 100°C). Another consequence of the anisotropy cancellation is the strong variation in losses with temperature. Thermal stability is good on the low temperature side of the SRT since loss decrease with T, but, in contrast, on the high temperature side, losses increase with T which in turn contribute to increase temperature. As a consequence if the cooling is not sufficient, there is a risk of thermal runaway. Losses of selected ferrites are given in Annex 1, Table 1.17 and compared with competing materials.

1.7.4 Ni-Zn ferrites

The simple nickel ferrite is an inverse spinel: this means that the Ni^{2+} ion goes in the octahedral site only. The effect of Zn substitution on intrinsic magnetic properties is very similar to that in MnZn ferrites, except that Ni gives lower magnetic moment ($2\,\mu_B$) and higher Curie point and anisotropy constant than Mn. This means that NiZn ferrites can be used at higher temperature than MnZn ones in general and that their permeability will be lower. Howerver, the great advantage is that Ni can be divalent only and iron trivalent only, so conduction by electron hopping is impossible. As a consequence, the resistivity is within the order of magnitude of $> 10^5\,\Omega$m. A very small excess of

Table 1.13. Main $Mn_{1-x}Zn_xFe_20_4$ materials used for power transformers and power electronics. References starting with a letter are from TDK, with a number from Ferroxcube.B_{1k} is the induction measured at 1 kAm^{-1}

ref.	x	B_{1k} (T)	B_{1k} (T)	μ_i	f_R (Hz)	H_C(A/m)	T_C (°C)	ρ (Ωm)	f_{max}(Hz)
	(approx)	25°C	100°C	± 30%		25°C			
N72	0.37	0.48	0.37	2500	20 M	23	210	12	300 k
N27	0.35	0.50	0.41	2000	15 M	33	220	3	150 k
N49	0.3	0.49	0.40	1500	30 M	42	240	17	1 M
3C93	0.3	0.52	0.43	1800	20 M	13	240	5	300 k
3F35	0.3	0.5	0.42	1400	50 M	40	240	10	1 M

Table 1.14. Main $Ni_{1-x}Zn_xFe_20_4$ materials. References starting with a letter are from TDK, with a number from Ferroxcube. B_{5k} is the induction measured at 5 kAm^{-1}

ref.	x (approx)	B_{5k} (T) 25°C	B_{5k} (T) 100°C	μ_i ± 30%	f_R (Hz)	H_C(A/m) 25°C	T_C (°C)	ρ (Ωm)	f_{max}(Hz)
K1	0.30	0.31	0.28	80	50 M	400	425	10^5	12 M
4C65	0.35	0.38	0.34	125	55 M	280	350	10^5	1 M
4B1	0.38	0.36	0.31	250	25 M	150	260	10^5	1 M
4A11	0.60	0.34	0.23	850	7 M	33	180	10^5	1 M
K10	0.65	0.32	0.24	800	4 M	165	115	10^5	1 M
4A20	0.72	0.26	0.15	2000	1.4 M	11	100	10^5	300 k

iron results in a spectacular drop in resistivity (6 orders of magnitude), it is thus usual to prepare the ferrite with a slight iron default (for example 1.96 instead of 2) in order to compensate iron pollution from steel balls and vial of the mill. NiZn ferrtites can be sintered in air (no control of the oxygen pressure needed) without prejudice of the magnetic or electrical properties. As a consequence, there is no need to introduce interfacial resistive oxide. The magnetic properties of NiZn ferrites are controlled by two parameters, the zinc content and the microstructure. As in MnZn ferrite, the Zn lowers the Curie point and by consequence the magnetocrystalline anisotropy and in turn enhances the permeability. Table 1.14 a clear correlation is seen between T_C and μ_i. Also the sintering temperature plays a role since it affect the grain size and the density (1.49). For example in order to have a large bandpass, 4C65 has low zinc content and is sintered at lower temperature to get low density (4500 $kg \cdot m^{-3}$, 86%) and small grain size. In contrast, to get a large permeabilty, 4A20 has high content of Zn and is sintered at higher temperature to get high density (5000 $kg \cdot m^{-3}$, 96%) and coarser grains.

1.7.5 Other soft ferrites

Ni-Zn-Cu ferrite

This familly of ferrite is basically issued from NiZn one. It was developed for the manufacturing of micro-inductances. A micro-inductance is a component made by co-sintering of a metallic coil embedded in ferrite (typically from $1 \times 0.5 \times 0.5$ mm to $2 \times 1.25 \times 1.25$ mm). This is realized by stacking bonded ferrites and silica tapes on which coils are printed. In principle noble metals (Pd, Pt) are compatible with ferrites but they are to expensive. As a consequence, the sintering temperature is decreased by substitution of copper to Ni to be compatible with silver (about 950°C).

The typical formula is $Ni_{1-x-y}Zn_xCu_yFe_20_4$, where $0.3 < Zn < 0.6$ and $0.1 < Cu < 0.2$. In principle, manufacturers provide properties of the components but not that of the material. However, properties of these ferrites are comparable to that of NiZn, i.e. a permeability in the range of several hundreds

with substantially lower magnetization [25]. Also Ni-Zn-Cu ferrites show very low loss at high frequency (about 300 mWcm^{-3} at 1.5 MHz, 25 mT) when a small amount of Co is substituted to Ni in order to produce a SRT close to room temperature [31, 32].

Microwave ferrites

The term microvawe usually refers to UHF to mm vawes (300 MHz to 300 GHz according to IEEE standard) but ferrites are used only below 110 GHz (W-band.) In microwave applications, the main quantity characterizing the material is not the permeability or the magnetization but the gyromagnetic resonance frequency. In soft magnetic materials, the anisotropy field is by definition low, so the main field is the dipolar field produced by the magnetization itself. As a consequence, the resonance frequency is mainly defined by

$$f_R = \frac{\gamma}{2\pi} J_S \tag{1.50}$$

where $\frac{\gamma}{2\pi} \simeq 28$ GHz/T. The working frequency is usually chosen in the vicinity of f_R, higher in the upper band, lower in the lower band. So from (1.50) it is clear that a low magnetization is necessary for UHF whereas a high one is needed in W-band. At constant frequency, the material shows an absorption peak (a maximum in μ'') as a function of the DC field. This absorption peak is characterized by its FWHM, ΔH expressed in A/m and is the main characteristic of microwave ferrites. Depending on the application, the line width ΔH should be sharp or large and can be tuned according to [28]:

$$\Delta H = \Delta H_i + \frac{3}{2\mu_0} p J_S + 2.07 \frac{\mu_0 K_1}{J_S^3} \tag{1.51}$$

Table 1.15. Properties of selected microwave ferrites [6, 30, 39]. For gadolinium-iron garnets the compensation point of the magnetization is indicated with the Curie point. The dielectric permittivity lies in the range 13-16.

Composition	J_S(T) 25°C	T_C (°C)	ΔH (kA/m)	frequency of use (GHz)
$NiFe_20_4$	0.34	585	32	10-40
$Ni_{0.6}Zn_{0.4}Fe_20_4$	0.5	350	13	10-40
$Li_{0.5}Fe_{0.5}Fe_20_4$	0.36	640	28	10-40
$Li_{0.3}Fe_{0.3}Zn_{0.4}Fe_20_4$	0.50	425	8	10-40
$Y_3Fe_50_{12}$	0.19	290	6	1-10
$Y_{1.5}Gd_{1.5}Fe_50_{12}$	0.096	-150/290	14	1-10
$Gd_3Fe_50_{12}$	0.009	27/290	broad	1-10
$Y_{2.4}Ca_{0.6}Fe_{4.7}V_{0.3}O_{12}$	0.122	235	4	1-10
$Y_{1.4}Ca_{1.6}Fe_{4.1}V_{0.8}O_{12}$	0.036	225	40	1-10
$Y_3Fe_{4.75}In_{0.25}O_{12}$	0.19	207	3	1-10
$Y_{1.8}Ca_{1.2}Fe_{3.8}V_{0.6}In_{0.6}O_{12}$	0.1	109	1	1-10

where the first term —due to gyromagnetic damping — is intrinsic (see chap. MRE, the second term corresponds to the broadening due to porosity (p), the last one is due to spin waves broadening (the factor 2.07 is for a sphere). Because porosity is not desirable, as it is detrimental to the losses, ΔH is tuned by adjusting J_S with substitutions. In non-reciprocal applications, such as gyrators or isolators, the DC field is constant and can be produced by a magnet. In reciprocal applications, a DC field is applied to the material by a permanent magnet and the microwave field is applied perpendicularly (or less commonly parallel in some applications). In tunable phase shifter, the field is of course variable and produced by an electromagnet. In applications exploiting the Faraday effect (rotation of the polarization plane), the ferrite is not polarized.

Microwave ferrites are of two types: spinels and garnets, there main characteristics are given in Table 1.15.

Microwave spinels are very similar to other soft ferrites except the substitution type or rate:

- NiZn microwave ferrites contains less Zn in general (between 0 and 0.3), they are cheapest microwave ferrites since they are massively produced for other purposes;
- magnesium ferrites, in which Mg is combined with Mn as divalent element, which exhibits lower loss than NiZn ones;
- lithium ferrite , where Li^+ is combined with trivalent iron according to the formula $(Li^+_{0.5}Fe^{3+}_{0.5})_{1-x}Zn_xFe_20_4$, which have sharper absorption line.

Among microvawe spinels, lithium one show the the best properties (small ΔH, high T_C, low loss) but they are much more difficult to produce since Li partly evaporates during firing.

Yttrium iron garnet (YIG) has the canonical composition ($Y_3Fe_50_{12}$ where all metal ions are trivalent. Here again, there are a lot of possible substitutions providing the ion has charge and ionic radius compatible with the crystallographic site in which it is supposed to go. Most common substitutions are:

- Al for Fe which reduced J_S for VHF/UHF applications
- Gd for Y which produce a compensation point [2] of the magnetization and a positive magnetization variation with temperature in a range tunable by the Gd content;
- a combination of Gd and Al to combine the above mention effects;
- Fe by In in order to increase the magnetization (using the same effect as Zn in spninels);
- Ca^{2+} is also substituted for Y when combined with V^{4+} to enhance the magnetization.

[2] The compensation point is the temperature at which magnetization of A and B site compensate see chapter MOX

YIG is the only magnetic material transparent to light (in the near infrared) and display strong Faraday effect , it is thus also used in magneto-optical devices. Due to its compensation point, Gd-YIG thermal variation of the saturation magnetisation is rather low around room temperature. Upon all microwave ferrites YIG has the lowest dielectric loss ($\tan\delta = 2 \cdot 10^{-4}$ at 8.2 GHz and ≈ 5 for spinels)

Microwave ferrites are produced using the same processes as spinel ferrite but in particular shapes: sphere (in the past), disk, square or triangle (usually with cut corners) from 0.5 mm to 3 mm thick and up to 50 mm large.

1.8 Effect of a gap on magnetic properties

Cores with gap are use in every application where inductive energy storage is necessary such as smoothing chokes or coupled inductors because most of soft magnetic material cannot store energy (except stress annealed Finemet and in a lower extend transverse field annealed amorphous alloys ans permalloy). Gaps can be either lumped or spread depending on the application.

1.8.1 Core with lumped gap

Core with lumped gap are made of any kind of soft magnetic materials depending essentially on the frequency of the device (silicon steel, Fe-Ni, Mn-Zn ferrite, amorphous...) They are exactly similar to single-phase transformer cores except the fact stacked-cores are stacked without overlapping joints and that tape wound cores are more frequently used. Rectangular tape wound core are cut into two pieces after impregnation (C-cores), whereas ring cores are moulded in resin before cutting a single gap. The effective permeability of the core (assuming a constant cross section area along flux lines) is expressed in a very similar way as (1.49):

Table 1.16. Magnetic properties of selected powder cores. ϕ is the filling factor, $\langle D\rangle$ is the mean grain size [9, 26]

Composition	μ_R	J_S (T)	B_{10k} (T)	H_C (A/m)	ϕ (%)	$\langle D\rangle$ (μm)	ρ (Ωm)	f_{max} (Hz)	loss	mW/cm^3
Carbonyl iron	11	1.6	0.15	1600	60	4-8	5.10^5	80 M	$\mathcal{P}^{25\mathrm{mT}}_{1\ \mathrm{MHz}}$	=550
Carbonyl iron	20	1.9	0.3	1600	70	< 10	1	60 M	$\mathcal{P}^{25\mathrm{mT}}_{1\ \mathrm{MHz}}$	=800
Iron	40	1.0	0.9	1200	45		1	2 M	$\mathcal{P}^{25\mathrm{mT}}_{100\ \mathrm{kHz}}$	=450
Iron	75	1.8	1.3	900	62		10^{-2}	100 k	$\mathcal{P}^{25\mathrm{mT}}_{100\ \mathrm{kHz}}$	=250
Iron	220	2.0	1.33	200	91	40	18.10^{-3}	200 k	$\mathcal{P}^{1\mathrm{T}}_{1\ \mathrm{kHz}}$	= 28
Iron	950	2.1	1.63	200	96	100	70.10^{-6}	20 k	$\mathcal{P}^{1\mathrm{T}}_{1\ \mathrm{kHz}}$	= 19
Mo-permalloy	14	0.57	0.03	400	72	60		9 M	$\mathcal{P}^{25\mathrm{mT}}_{100\ \mathrm{kHz}}$	= 73
Mo-permalloy	160	0.74	0.2	400	92	200		700 k	$\mathcal{P}^{25\mathrm{mT}}_{100\ \mathrm{kHz}}$	= 37
Mo-permalloy	550	0.76	0.47	400	95	200		90 k	$\mathcal{P}^{25\mathrm{mT}}_{100\ \mathrm{kHz}}$	=266

$$\mu_{eff} = \frac{\mu_R}{1 + \mu_R \frac{\sigma g}{\ell}} \tag{1.52}$$

where g is the length of the gap, ℓ the length of the magnetic path and σ is the dispersion coefficient due to flux spreading in the gap. For small gaps, i.e. when g is small compared to ℓ and to the dimensions of the cross section, $\sigma \simeq 1$. If this condition is not realized, $\mu_{eff} = \frac{\ell}{\sigma g}$ and σ is usually smaller than 0.5. The advantage of lump gap core is the possibility to tune the permeability by the user. However, flux leakage around the gap is responsible for electromagnetic emission and additional losses due to the non uniformity of the induction at the gap edges.

1.8.2 Cores with spread gap

Cores with spread gap are used to overcome the drawbacks of lumped cores especially in the RF bands. They are realized from metallic powders mixed with a resin and pressed. The filling factor is adjusted to the target permeability The effective permeability can be expressed as a function of the filling factor, ϕ, the volume ratio occupied by ferromagnetic particles in the core:

$$\mu_{eff} = \frac{\mu_R}{1 + \mu_R(1 - \phi^{1/3})} \tag{1.53}$$

for large concentrations, or for low concentrations satisfying $\mu_R(1 - \phi) \gg 3$ by Clausius-Mosotti formula

$$\mu_{eff} = \frac{1 + 2\phi}{1 - \phi} \tag{1.54}$$

The main advantages of powder core compared to lumped gap cores are lower losses for a given effective permeability and the possibility to shape cores by pressing or injection moulding in the form of rings, E, L, screws, pots, cups, tubes, rods...

Iron powder cores

Iron powder are used for high frequency because of the of large magnetization and magnetocrystalline anisotropy which pushes the ferromagnetic resonance above 1 GHz. For frequencies above 10 MHz, particles have to be smaller than 10 μm to limit eddy currents. Iron carbonyl particles are made by decomposition of $Fe(CO)_5$. They contain impurities due to the process (O, N, C) which contributes to increase the permeability. They have a grain size distribution between 1 and 10 μm and an oxide surface layer. Due to the small grain size, the particle permeability is small according to (1.47) and the filling factor is low, so the effective permeability is maximum 20 in practice.

For higher permeabilities, different methods for pure iron particles production can be used, but the most efficient are atomization in inert gas or

rotating electrode sputtering because these techniques give powder with good sphericity and low size dispersion. The permeability depends on the size of the particles (usually from several tens to about 200 μm), the binder quantity, the pressure and the temperature of compaction. Depending on the filling factor and the grain size, the permeability extends from several tens to nearly 1000. Of course, as ϕ increases, the resistivity drops due to contact between particles and percolation (see Table 1.16).

Iron powder cores are used in a great variety of applications, from power components in RF radio emitters, to HF power electronics. High density hot pressed powder cores, aka soft magnetic composites (SMC), exhibits permeabilities between 200 and 1000, they are used for chokes and electrical motors respectively.

Mo-permalloy powder cores

Molybdenum permalloy powders cores, aka MPP, are made by the same methods as the pure iron ones. They have larger permeability for the same filling factor and lower losses for the same perm eabilty due to the vanishing magneto-crystalline anisotropy. On the other side, they have lower band pass due to the smaller J_S and K_1. MPP are used for high frequency power electronics as smoothing chokes, resonance inductor, inverter inductors or fly-back SMPS coupled inductor.

Other powder cores

Besides the above mentioned common powder core, there are also niche markets for more exotic materials:

- $Fe_{50}Ni_{50}$, is a compromise between high B iron and low loss MPP, for $\mu_R = 160$, $\mathcal{P}^{25\mathrm{mT}}_{100\ \mathrm{kHz}} = 70\ \mathrm{mWcm}^{-3}$;
- Sendust is an iron alloy containing 9% Si 6% Al, a composition very close to the ordered $Fe_3(Si, Al)$, that shows characteristics quite similar MPP (K_1 and $\lambda_S \simeq 0$) but with higher magnetization (up to 1 T), for $\mu_R = 160$, $\mathcal{P}^{25\mathrm{mT}}_{100\ \mathrm{kHz}} = 30\ \mathrm{mWcm}^{-3}$;
- 6.5 silicon steel is also used for its zero magnetostriction (low noise in the audio band like MPP or Sendust) but with higher losses and lower permeability due to non-zero K_1.

References

1. Behzad Ahmadi, Zehani, Karim, Martino LoBue, Vincent Loyau, and Mazaleyrat, F. Temperature dependence of magnetic behaviour in very fine grained, spark plasma sintered NiCuZn ferrites. *Journal of Applied Physics*, 111(7):07A510, April 2012.
2. R. Alben, J. J. Becker, and M. C. Chi. Random anisotropy in amorphous ferromagnets. *J. Appl. Phys.*, 49:1643, 1978.

3. F Alves, F Simon, SN Kane, Mazaleyrat, F., T Waeckerle, T Save, and A Gupta. Influence of rapid stress annealing on magnetic and structural properties of nanocrystalline fe 74.5 cu 1 nb 3 si 15.5 b 6 alloy. *Journal of Magnetism and Magnetic Materials*, 294(2):e141–e144, 2005.
4. J-B; Hérission D; Benchabi A; Waekerlé T; Fraisse H; Boulogne B Alves, F; Desmoulin. Nanocrystalline material strip production for the formation of magnetic torus comprises annealing cast amorphous ribbon of specified composition defiling under tension, 2002.
5. Amperam. *Nanocrystalline Core Solution*, 2012.
6. Elmer E Anderson, J Richard Cunningham Jr, and GE McDuffie. Magnetic properties of the mixed garnets (3- x) y 2 o 3· x gd 2 o 3· 5 fe 2 o 3. *Physical Review*, 116(3):624, 1959.
7. Carlo Appino, Mahmood Khan, Olivier de la Barrière, Carlo Ragusa, and Fausto Fiorillo. Alternating and rotational losses up to magnetic saturation in non-oriented steel sheets. *IEEE Transactions on Magnetics*, 52(5):1–4, 2016.
8. Edoardo Barbisio, Fausto Fiorillo, and Carlo Ragusa. Predicting loss in magnetic steels under arbitrary induction waveform and with minor hysteresis loops. *IEEE Transactions on Magnetics*, 40(4):1810–1819, 2004.
9. BASF. *Carbonyl Iron Powder for Inductive Electronic Components*.
10. Cinzia Beatrice, Carlo Appino, Olivier de la Barrière, Fausto Fiorillo, and Carlo Ragusa. Broadband magnetic losses in fe-si and fe-co laminations. *IEEE Transactions on Magnetics*, 50(4):1–4, 2014.
11. G. Bertotti. *Hysteresi in magnetism*. Academic Press, San Diego, 1998.
12. Giorgio Bertotti. General properties of power losses in soft ferromagnetic materials. *IEEE Transactions on magnetics*, 24(1):621–630, 1988.
13. Giorgio Bertotti. Dynamic generalization of the scalar preisach model of hysteresis. *IEEE Transactions on Magnetics*, 28(5):2599–2601, 1992.
14. Giorgio Bertotti and Isaak D Mayergoyz, editors. *The Science of Hysteresis: Physical modeling, micromagnetics, and magnetization dynamics*. Academic Press, 2006.
15. Fred Brailsford. *Physical principles of magnetism*. London, 1966.
16. A Cazin. Sur les effets thermiques du magnétisme. *J. Phys. Theor. Appl.*, 5(1):111–118, 1876.
17. O. de la Barriere, C. Ragusa, C. Appino, F. Fiorillo, M. LoBue, and Mazaleyrat, F. A computationally effective dynamic hysteresis model taking into account skin effect in magnetic laminations. *Physica B-Condensed Matter*, 435:80–83, FEB 15 2014.
18. J. A. Ewing. *Induction in iron and other metals*. The Electrician, 2^{nd} edition edition, 1901.
19. A.A. Glaser, N.M. Kleynerman, V.A. Lukshina, A.P. Patapov, and V.V. Serikov. Thermomechanical treatment of the nanocrystalline alloy fecunbsib. *Phys.Met. Metal.*, 72:53, 1991.
20. G. Herzer. Grain structure and magnetism of nanocrystalline ferromagnets. *IEEE Trans. Magn.*, 25:3327–29, 1989.
21. G. Herzer. Grain size dependence of coercivity and permeability in nanocrystalline ferromagnets. *IEEE Trans. Magn.*, 26:1397–1402, 1990.
22. Hitachi Metals. *Metglas amorphous alloys*.
23. Hitachi Metals. *Nanocrystalline soft magnetic material FINEMET*, 2006.
24. JFE Steel Corporation. *JFE Super Core (Electrical steel sheets for high-frequency application)*, 2005.

25. Richard Lebourgeois, Sonia Duguey, Jean-Pierre Ganne, and Jean-Marc Heintz. Influence of v 2 o 5 on the magnetic properties of nickel–zinc–copper ferrites. *Journal of Magnetism and Magnetic Materials*, 312(2):328–330, 2007.
26. Micrometals. *Arnold powder cores*.
27. Orb Electrical Steels. *Cogent™Non oriented electrical steel, typical data*, 2015.
28. C Patton. A review of microwave relaxation in polycrystalline ferrites. *IEEE Transactions on Magnetics*, 8(3):433–439, 1972.
29. RH Pry and CP Bean. Calculation of the energy loss in magnetic sheet materials using a domain model. *Journal of Applied Physics*, 29(3):532–533, 1958.
30. MH Sirvetz and JE Zneimer. Microwave properties of polycrystalline rare earth garnets. *Journal of Applied Physics*, 29(3):431–433, 1958.
31. Lucas, A., R. Lebourgeois, Mazaleyrat, F., and E. Laboure. Temperature dependence of spin resonance in cobalt substituted NiZnCu ferrites. *Applied Physics Letters*, 97(18):182502, November 2010.
32. Lucas, A., R. Lebourgeois, Mazaleyrat, F., and E. Laboure. Temperature dependence of core loss in cobalt substituted Ni-Zn-Cu ferrites. *Journal of Magnetism and Magnetic Materials*, 323(6):735–739, March 2011.
33. Mazaleyrat, F. and L. K. Varga. Thermo-magnetic transitions in two-phase nanostructured materials. *IEEE Transactions On Magnetics Transactions On Magnetics*, 37(4):2232–2235, July 2001.
34. ThyssenKrupp Electrical Steel GmbH. *Grain oriented electrical steel PowerCore®*, 2012.
35. Hiroaki Toda, Yoshihiko Oda, Masaaki Kohno, Masayoshi Ishida, and Yoshiaki Zaizen. A new high flux density non-oriented electrical steel sheet and its motor performance. *IEEE Transactions on Magnetics*, 48(11):3060–3063, 2012.
36. Takanori Tsutaoka. Frequency dispersion of complex permeability in mn–zn and ni–zn spinel ferrites and their composite materials. *Journal of Applied Physics*, 93(5):2789–2796, 2003.
37. Vacuumschmelze. *Soft Magnetic Materials and Semi-finished Products*, 2005.
38. Emil Warburg. Magnetische untersuchungen. *Annalen der Physik*, 249(5):141–164, 1881.
39. R. G. WEST and AC Blankenship. Magnetic properties of dense lithium ferrites. *Journal of the American Ceramic Society*, 50(7):343–349, 1967.
40. Y. Yoshizawa and K. Yamaguchi. New Fe-based soft magnetic alloys composed of ultrafine grain structure. *J. Appl. Phys.*, 64:6044, 1988.

Annex 1: Application of soft magnetic materials

Table 1.17. Comparison of losses in different magnetic material used in power electronics. All values are indicated for the same $B \times f = 25$ kVm^{-2}

B (mT)	1000	250	100	50	25	10	5
f (kHz)	25	100	250	500	1000	2500	5000
3C93		1000	800	300			
3F35				80	120		
4F1						100	80
N27		1400	1000				
N49		1000	300	120	80		
N72		400					
MP205		7000	6000	6000			
Sendust160		4000	2700	2000			
2714A		683	759				
Finemet	1900	759					

Annex 2: Application of soft magnetic materials

Table 1.18: In the following table, different classes of applications are reviewed and materials are proposed for the purpose. These propositions are only guide lines, the grade must be adapted to the application specifications (frequency, shape, cost...) VH stands for very-high, H for high, VL for very low and L for low

Application	Required properties	Material type	Typical grade
Network transformer	H B, VL 50 Hz loss	GO Fe-Si	M090-23P
HV/LV Network transformer	H B, VL 50 Hz loss loss	Fe-based glass	Metglas SA
	H B, VL 50 Hz loss	GO Fe-Si	M110-27S
LV industrial transformer	H B, L 50 Hz loss	GO Fe-Si	M110-35-N
Airborne transformer	VH B	Fe-Co	49%Co
Household transformer	L cost	L Si steel	M600-50-A
Power station generator stator	H B, VL loss	GO Fe-Si	M090-30-N
Power station generator rotor	strength	forged steel	95%Fe+Ni, Cr, Mo, C
Boat/train motors	H B, L loss	NO FeSi	M235-35-A
Industrial motors	H B, L 50 Hz loss	NO FeSi	M330-35-A
High speed motors	H B, L VF-band loss	NO FeSi	M270-20-A
Automobile motors	H B, VL loss	NO FeSi	M210-27-A
Automobile generators	H B, L cost	NO FeSi	M400-50-A
Claw pole rotor	forgeability	C steel	C05E
Airborne generators	VH B, strength	FeCo	25%Co
Electromagnetic motor valve	VH B	FeCo	49%Co
Household AC motors	L cost	L Si steel	M600-50-A
Small DC motor stator	stampability	steel	low C
Small DC motor rotor	L cost	L Si steel	M600-50-A
Watch step motor	H B and μ	Fe-Ni	50%
Inductive Encoders		Fe-Ni	50%

Continued on next page

Table 1.18: continued from previous page

Application	Required properties	Material type	Typical grade
Forward SMPS transformer	L 10kHz loss	Amorphous	Co-based
		Co-based	F loop
		nanocryst.	F loop
		MnZn ferrite	power grade
Flyback SMPS transformer	$B_R = 0$, L μ	MnZn ferrite	power grade+gap
		nanocrystalline	stress annealed
Smoothing choke	linearity, f<10 kHz	FeSi	wound core+gap
	linearity, f<100 kHz	MnZn	gap
	linearity, f<100 kHz	powder core	MPP or iron
	linearity, f<100 kHz	nanocrystalline	stress annealed
	linearity, f>100 kHz	carbonyl iron	
Resonance SMPS	L LF-band loss	MnZn ferrite	power grade
		powder core	MPP
	L MF-band loss	NiZn ferrite	power grade
		MPP	carbonyl iron
Wideband transformer	H μ		signal grade
Drive transformers for IGBT	H μ, linearity	FeNi	field annealed permalloy
Drive transformer for GTO	H B_R, H dynamics	FeNi	textured 50%Ni
Network inductor	H B	GO FeSi	N-grade wound core + gap
Pulse transformer	H B_R, H dyn.	Co amorphous	Z loop
Spike killer	H B_R, H dyn.	Co amorphous	Z loop
Delay lines	H μ, bar shape	MnZn ferrite	signal grade
Magnetic amplifier	H B_R	GO FeSi	N-grade wound core
Current transformer	H μ	permalloy	F loop
		Co amorphous	F loop
		nanocryst.	F loop
Thick layer micro-inductor	low sintering temp.	Ni-Zn-Cu ferrite	tape casting
On-ship inductance	integration	YIG	RF sputtered on substrate
On-ship transformer	H μ	Fe-Ni	electrodeposited
Flux-gate sensor	VH B_R, VL H_C	Co amorphous	F loop
Hall effect sensors	L B_R, L H_C	MnZn ferrite	signal grade
Magnetostrictive sensor	Hλ_S	Amorphous	Fe/FeNi based
Proximity sensors	H MF-band μ	MnZn ferrite	
Ground fault circuit breaker	VH μ	Co amorphous	F loop
		nanocryst.	F loop
		FeNi	permalloy
Common mode filter	VH μ	MnZn ferrite	signal grade
		nanocrystalline	field annealed
LF filter	L μ	MnZn ferrite	signal grade + gap
MF-UHF filter	L μ	NiZn ferrite	
Telecom transformer	H μ	MnZn ferrite	signal grade
LF antenae	linearity, high μ	MnZn ferrite	
MF antenae	bandwidth	NiZn ferrite	$\mu < 1000$
HF antenae	bandwidth	NiZn ferrite	$\mu < 250$
VHF antenae	bandwidth	NiZn ferrite	$\mu < 100$
UHF antenae	bandwidth	NiZn	$\mu < 20$

Continued on next page

Table 1.18: continued from previous page

Application	Required properties	Material type	Typical grade
Radar absorber	UHF absorption	NiZn	plate, structured surface
Faraday effect uniline	$H_C < 100$A/m	Li ferrite	rod
Resonator filter	L loss, L ΔH	(Ga)YIG	single crystal sphere
Circulator, phase shifter	$f < 1.5$ GHz	Gd-YIG	plate, rod
	$1.5 < f < 10$ GHz	Al-YIG	id.
	$f > 10$ GHz	Li or NiZn spinel	id.
Wireless energy transfer	H B, L MF-band loss	ferrite	MnZn
Zero telsa chamber	H μ	FeNi	mumetal
MF Magnetic shielding		MnZn ferrite	signal grade
Flexible magnetic shielding	H μ	nanocrystalline	polymer film
	large bandwidth	MnZn ferrite	powder in polymer film
Induction cooking pan	controlled T_C	FeNi	thermal alloy
DC electromagnet	H B	iron	bulk
AC electromagnet	H B	FeSi	M600-100-A

Index